Plant Physiology and Biochemistry 238 (2026) 111680

Contents lists available at ScienceDirect

Plant Physiology and Biochemistry

journal homepage: www.elsevier.com/locate/plaphy

Distinct root signaling and anatomy associate with convergent leaf responses to drought and salinity in grapevine rootstocks

Sara Anichini [a], Sara Parri [b], Andrea Bellini [b], Claudia Faleri [b], Marco Romi [b], Luigi Falginella [c], Elisa De Luca [c], Giampiero Cai [b,*]

[a] Department of Agriculture, Food, Environment and Forestry (DAGRI), University of Florence, Piazzale delle Cascine 18, Florence, 50144, Italy
[b] Department of Life-Sciences, University of Siena, Via Mattioli 4, Siena, 53100, Italy
[c] VCR Research Center, Via Ruggero Forti 4, San Giorgio della Richinvelda, 33095, Italy

ARTICLE INFO

Keywords:
Grapevine
Rootstock
Drought stress
Salt stress
Gas exchange
Zeaxanthin epoxidase
ABA
Aeroponic system

ABSTRACT

Drought and salinity seriously threaten grapevine productivity by inducing convergent leaf phenotypes through distinct upstream signals. This study investigated how abscisic acid (ABA) dynamics, root anatomical traits and zeaxanthin epoxidase (ZEP) content influence tolerance strategies in five rootstocks (140 Ruggeri, Kober 5BB, Dog Ridge, M2 and M4) grown in an aeroponic system. Our results reveal that, although both stresses drastically reduce stomatal conductance and net CO_2 assimilation, the underlying signalling pathways diverge radically. Drought was closely associated with genotype-dependent accumulation of leaf ABA and increased immunoreactivity of the 65-kDa ZEP band in roots. This was accompanied by marked endodermal suberisation, particularly in M2, M4 and Kober 5BB, favouring a water conservation strategy. In contrast, salinity induced similar physiological declines with minimal ABA induction (except for the high basal levels in 140 Ruggeri), suggesting the dominance of non-hormonal osmotic, ionic and hydraulic constraints. Furthermore, while drought primarily affected water status, salinity triggered plastic remodelling of biomass with increased allocation to the roots. This study demonstrates that leaf phenotypic convergence can mask divergent control architectures modulated by root anatomical traits. These traits help distinguish between water-conservative and water-spending behaviours and provide critical parameters for identifying genotypes with enhanced resilience to environmental stress.

1. Introduction

Abiotic factors such as drought and salinity present significant challenges to plants in warm regions by limiting the opening of stomata and reducing the assimilation of carbon (Gambetta et al., 2020; Meggio et al., 2014; Munns and Tester, 2008; Zhang et al., 2016). While both stresses frequently induce convergent leaf phenotypes, such as early stomatal closure, reduced net photosynthesis, and altered photosystem II efficiency, it remains unclear whether these similar outcomes arise from shared or distinct signaling and root structural mechanisms across genotypes (Gambetta et al., 2020; Meggio et al., 2014).

The grapevine is a perennial plant in which the use of different rootstocks enables the analysis of signalling mechanisms in response to stressful conditions. Grapevine rootstocks exhibit significant genetic variability in stress tolerance which is regulated by physiological mechanisms such as abscissic acid (ABA)-mediated stomatal control, aquaporin expression and root architecture plasticity (Marín et al., 2021; Prinsi et al., 2021). The most well-known tolerant rootstocks to both stresses are 1103 Paulsen, 140 Ruggeri and Ramsey, which are effective at excluding toxic ions and maintaining cell turgor (Mustapha et al., 2025; Zhou-Tsang et al., 2021). Conversely, 101-14 MGt and Riparia Gloire rootstocks are classified as highly sensitive (Khan et al., 2020; L. Zhang et al., 2016). Recently, the M4 genotype has emerged due to its superior ability to acclimatise and maintain photosynthesis under severe stress (Lucini et al., 2020; Meggio et al., 2014).

In grapevines, ABA mediates long-distance signalling during progressive water deficit (Marusig and Tombesi, 2020), promoting stomatal closure and water conservation. Rootstocks modulate the balance between water-conserving (isohydric) and water-spending (anisohydric) strategies by regulating hormone dynamics and hydraulic properties (Bianchi et al., 2023; Dargie et al., 2014; Koundouras et al., 2008; Labarga et al., 2023; Lovisolo et al., 2010; Marguerit et al., 2012; Vandeleur et al., 2009). Genetic studies further linked ABA signalling with stomatal regulation and drought-related metabolic adjustments,

* Corresponding author.
E-mail address: cai@unisi.it (G. Cai).

https://doi.org/10.1016/j.plaphy.2026.111680
Received 16 April 2026; Received in revised form 7 August 2026; Accepted 21 August 2026
Available online 22 August 2026

such as raffinose synthesis (Pizzio et al., 2024). Together, these findings suggested a mechanistic link between leaf hormonal changes and carbon assimilation during drought (Pizzio et al., 2024); however, whether this signalling logic extends to salinity stress remains unclear.

Under salinity, gas exchange limitations occur with minimal ABA induction, implicating osmotic, hydraulic and ionic constraints. ABA contribution varies across genotypes, while ion exclusion/compartmentation and osmotic-hydraulic effects dominate (Meggio et al., 2014; Munns and Tester, 2008). This divergent upstream control may explain how distinct signalling architectures produce similar downstream leaf phenotypes in response to different stress (Gambetta et al., 2020; Meggio et al., 2014).

In addition to hormones, root anatomy may influence responses to drought and salinity by regulating radial and axial movement of water and solutes. Anatomical remodelling, such as endodermal suberisation, modifies hydraulic and ionic filtering, while diameter and density of xylem vessels influence cavitation resistance and transport capacity traits that vary among grapevine rootstocks to influence stress strategies (Alonso-Forn et al., 2025; Barrios-Masias et al., 2015; L. Zhang et al., 2016). Despite widespread rootstock use, how genotypes integrate hormonal and anatomical responses remains unclear, likely due to variations in scion/rootstock combinations, plant developmental stages, and assessment criteria (Alonso-Forn et al., 2025; Bianchi et al., 2023; Marguerit et al., 2012; Ollat et al., 2015).

This study evaluated i) whether responses in aeroponically-grown grapevines mirror those observed in soil, facilitating the soil-independent study of stress, ii) whether similar leaf phenotypes originate from distinct regulatory mechanisms across five rootstocks, and iii) whether drought and salinity trigger different root-level responses despite inducing comparable leaf physiology. We hypothesized that drought stress induces genotype-dependent increase in leaf ABA aligned with stomatal closure and photosynthetic downregulation (Koundouras et al., 2008; Labarga et al., 2023; Lovisolo et al., 2010; Trenti et al., 2021; Vandeleur et al., 2009). Conversely, despite lower ABA induction, salinity is hypothesized to limit gas exchange, driven primarily by osmotic, hydraulic, and ionic constraints (Meggio et al., 2014; Munns and Tester, 2008). Finally, root endodermal suberisation and xylem traits are predicted to shape leaf stress responses by influencing water-conservative versus water-spending stress strategies (Alonso-Forn et al., 2025; Barrios-Masias et al., 2015; L. Zhang et al., 2016).

Understanding rootstock drought and salinity tolerance requires investigating how anatomical traits contribute to stress resilience (Bianchi et al., 2023; Dargie et al., 2014; Koundouras et al., 2008; Meggio et al., 2014; Zhang et al., 2016) as the physiological impact of root anatomical adjustments remains unclear (Alonso-Forn et al., 2025; Barrios-Masias et al., 2015; Cuneo et al., 2021; Fichtl et al., 2023). Although belowground processes are difficult to access, aeroponics enables direct observations and analysis of root responses by overcoming soil-related limitations (Lin et al., 2024; Tafesse et al., 2021). Consequently, this allows more reliable comparisons of drought- and salinity-induced responses across genotypes (Atkinson et al., 2019; Fichtl et al., 2023). When combined with physiological and molecular measurements, aeroponics facilitates the study of root-to-shoot signalling, root anatomy and hormone dynamics independently of soil heterogeneity (Moshelion et al., 2024; Tafesse et al., 2021; Tramontini et al., 2013).

2. Materials and methods

2.1. Plant material and rooting

The vine rootstock cuttings shown in Table 1 were obtained from Vivai Cooperativi Rauscedo (San Giorgio della Richinvelda, Italy - https://www.vivairauscedo.com/). After a 24-h rehydration period, the basal one-node of 15-20 cm cuttings were treated with a 0.3% (3000 ppm) indole-3-butyric acid (IBA, Merck, Rahway, New Jersey, USA) solution for 15 min before being transplanted into an aeroponic system showed in Fig. S1 (Santa Chiara Lab, University of Siena, Italy https://santachiaralab.unisi.it/it/strutture/farming-lab) for rooting and leaf production.

Table 1
Genetic background and tolerance characteristics to abiotic stress of the grapevine rootstock genotypes used in this study.

Genotype	Genetic background	Tolerance characteristics
140 Ruggeri	*V. berlandieri* x *V. rupestris*	**Water deficit** Higher root hydraulic conductance and lower vessel embolization; deeply developed root systems (Chen et al., 2024; Lovisolo et al., 2010) **Salinity** High Cl^- exclusion capacity (Tregeagle et al., 2010)
Kober 5BB	*V. berlandieri* x *V. riparia*	**Water deficit** High vigour but low tolerance of adverse soil conditions (Y. Chen et al., 2024) **Salinity** Salt-sensitive (J. Zhang et al., 2026); physiological and molecular mechanisms underlying salt tolerance remain poorly documented
Dog Ridge	*V. rupestris* × *V. candicans*	**Water deficit** High water use efficiency (Jogaiah et al., 2014) **Salinity** Cl^- exclusion capacity under salinity (Zhou-Tsang et al., 2021)
M2	cv. *Cosmo 10* x cv. *140 Ruggeri*	**Water deficit** Water-conservative strategy with low stomatal conductance, reduced transpiration, and high intrinsic water use efficiency (Dattola et al., 2026) **Salinity** Strong growth resilience under salinity stress and a good capacity for ionic homeostasis (Rius-Garcia et al., 2025)
M4	parent not confirmed, as described by Migliaro et al. (2019)	**Water deficit** Water spending strategy with high gas exchange rate and osmotic adjustment (Meggio and Pitacco, 2016) **Salinity** Contradictory literature: salt-tolerant in Meggio and Pitacco (2016); salt-sensitive in Rius-Garcia et al. (2025)

2.2. Growth conditions and stress application

Approximately 800 plants (around 160 per genotype) were selected to ensure they were at a similar and comparable developmental stage randomly divided into two groups: one for the water deficit treatment and one for the salt treatment. The 400 plants in each experimental group were then split into two subgroups: one with 200 control plants and one with 200 stressed plants. Each subgroup was irrigated via an independent irrigation line controlled by a separate NidoPro system (see below). This system enabled water and nutrients to be recirculated among several tanks, each of which held 40 plants. Tanks on the same irrigation line were therefore considered experimentally equivalent. The plants in the water-deficit experimental group were grown in the aeroponic system for 60 days before stress was applied, whereas the plants in the salt group were grown for 90 days before stress application. This was required because the aeroponic system could not handle two stress applications at the same time. Nevertheless, both the water-deficit and salinity experiments were conducted alongside their respective control groups, thereby ensuring that each stressed plant was compared to plants at the same stage of development. The aeroponics chamber was kept at 23 ± 2°C, 60% RH and an ambient CO_2 concentration around

400 ppm. The experimental lighting conditions were maintained with a photoperiod of 16 h of light and 8 h of dark, and a constant average Photosynthetic Photon Flux Density (PPFD) of ~200 μmol m^{-2} s^{-1} at canopy height across the tanks, with a red:blue (R:B) light ratio set to 75:25. The irrigation systems consisted of closed-loop water circuits, with drained water returning to the main tank; pH and EC were continuously monitored (NidoPro® fertigator, LogicSun, Cattolica, RN, Italy). The nutrient solution was Hoagland's solution (composition in Supplementary Material, Table S1) (electrical conductivity (EC) = 1.3 dS/m ± 0.2; pH = 5.5 ± 0.2) and was delivered to the roots via periodic nebulisation in 500 ml pulses per tank every 60 min for 40 s. Each aeroponic tank had a volume of 0.092 m^3.

Water deficit treatment was imposed by stepwise reduction of misting pulse duration and frequency in the closed-loop aeroponic system (full schedule in Supplementary Material, Table S2). This stepwise reduction in water availability was used to induce controlled water deficit while avoiding acute plant desiccation. Salt stress was applied by daily increments of NaCl up to 100 mM (Qin et al., 2016) over 10 days (EC trajectory in Supplementary Material, Table S2). Solution pH and EC were logged, with electrical conductivity (EC) of the solution increasing proportionally, from approximately 1.5 ± 0.5 dS m^{-1} at the start of the treatment to about 8.0 ± 0.5 dS m^{-1} at the final NaCl level.

2.3. Gas exchange measurements and chlorophyll fluorescence

For gas-exchange/fluorescence measurements, the first fully expanded leaf from the apex of the main shoot was chosen in each plant (n = 5) per genotype × treatment × timepoint. Leaf gas exchange and chlorophyll fluorescence parameters were assessed using a LI-6800 portable photosynthesis system equipped with a leaf chamber fluorometer (LICOR, Lincoln, NB, USA). We measured the light-saturated net photosynthetic rate (A), stomatal conductance (g_{sw}), electron transport rate (ETR), and photosystem II actual efficiency (ΦPSII). Measurements were conducted under controlled conditions within the leaf cuvette: photosynthetic active radiation (PAR) at 2000 μmol m^{-2} s^{-1}, CO_2 concentration at 400 ppm, block temperature at 26°C, and relative humidity at 60%. The maximum quantum yield of PSII (F_v/F_m), i.e. the maximum efficiency with which PSII converts absorbed light energy into photochemistry when all reaction centers are open, was also measured after dark adaptation (leaves were covered with aluminum foil for at least 20 min (Hajizadeh Sisakhti et al., 2025)). Physiological measurements were taken every 48–72 h during the water deficit treatment. Measurements were taken 24 h after the addition of 20, 40, 60, 90 and 100 mM NaCl during the salt stress period.

2.4. Fresh weight (FW), dry weight (DW) and water content (WC)

Leaves and roots from three plants were sampled separately for each experimental group. The samples were weighed immediately to determine their fresh weight (FW) and again after being heated in an oven at 60°C for 48 h to determine their dry weight (DW). Water content (WC) was determined using following formulas (Degenkolbe et al., 2009):

$$WC\ (g_{water} / g_{DW}) = \frac{(FW - DW)}{DW}$$

2.5. Analysis of abscisic acid

Approximately 500 mg of the first fully expanded leaf was ground to a fine powder in liquid nitrogen from a pool of three randomly chosen control plants and three drought/salt-stressed plants at timepoint 1. This was then extracted according to the instructions in the ABA quantification kit (Agrisera, Vännäs, Sweden, code AS204392). ABA was quantified via competitive ELISA using a 7-point calibration curve (0–10 μg mL^{-1}; R^2 = 0.9748); samples were read in triplicate using an Multiscan SkyHigh Plate Reader (Thermo Fisher Scientific, Waltham, MA, USA) and all readings fell within the standard curve range. The data were normalized to FW (μg g^{-1}).

2.6. Root histology

Roots were collected at random from three plants of each genotype. One-centimetre segments were then cut from each plant, 2 cm down from the root apex. These were then fixed immediately in a solution of 3% glutaraldehyde in 0.1 M cacodylate buffer (pH 7.2) for 2 h. The segments were then washed three times for 10 min each, dehydrated in ethanol solutions at concentrations of 10%, 30%, 50%, 70% and 100%, and finally immersed in a solution of alcohol and resin (JB-4, Electron Microscopy Sciences, Hatfield, PA, USA) and kept in the dark with slight agitation, increasing the resin volume gradually (3:1, 1:1, 1:3, pure resin). Samples were embedded in resin and polymerised at 4°C/24 h (Parri et al., 2024). Cross sections (3 μm) were stained with Toluidine Blue O (0.05% in benzoate buffer pH 4.0, 1 min). For suberin analysis, 3 μm sections were stained with 0.01% Fluorol Yellow 088 following the modified method of Brundrett et al. (1991). The stained samples were then rinsed quickly in 50% ethanol and dH_2O, and mounted in Citifluor (Agar Scientific). Root sections after histological staining were imaged using a Zeiss inverted microscope (Axiovert 5), 10×/NA, Axiocam 208 Color camera; images were acquired with Zeiss Zen 3.8 software. To analyse Fluorol Yellow staining, images of root sections were acquired using a Zeiss Axio Imager fluorescence optical microscope equipped with 10x and 63x objectives. An AxioCam MRm camera, managed by AxioVision software (Zeiss), was used for image acquisition with an excitation/emission wavelength of 470/525 nm.

Three images of each root section, all in the same position, were loaded into the ImageJ software (https://imagej.net/ij/), after which the following parameters were measured: total root area, stele area, cortex area, pericycle thickness, and the ratios of stele area to total area and cortex area to stele area. Calibration was performed using the scale bars provided by the Zeiss Zen 3.8 software.

2.7. Protein extraction and immunoblotting

At time point 1, samples of roots and leaves were collected from three different plants for genotyping and protein analysis. Proteins were extracted from leaf and root samples following the method of (Wu et al., 2014), with modifications from Parri et al. (2024). For each experimental group, three 0.3 g samples of either leaves or roots were ground in liquid nitrogen. Proteins were precipitated with 1.8 mL of cold 10% TCA/acetone solution containing 10 mM DTT for 20 min at −20°C. Following centrifugation at 15,000 × g for 5 min at 4°C, pellets were washed three times with 80% cold acetone, air dried for approximately 40 min, and resuspended in 0.8 mL SDS extraction buffer (1% SDS, 0.15 M Tris-HCl pH 8.8, 1 mM EDTA, 0.7 M sucrose, 1 mM DTT) supplemented with protease inhibitors. Samples were incubated at room temperature for 1 h with gentle agitation. After centrifugation (15,000 × g, 10 min), supernatants were transferred to new tubes and mixed with an equal volume of Tris-buffered phenol (pH 7.8-8.0), vortexed, and centrifuged (15,000 × g, 10 min, 4°C). The upper phenolic phase was collected and mixed with 4 vol of 0.1 M ammonium acetate in methanol, vortexed, and stored at −20°C for 2 h. Proteins were pelleted by centrifugation (15,000 × g, 10 min, 4°C), washed with 0.1 M ammonium acetate in methanol and then with 80% acetone. After air-drying, the protein pellets were resuspended in an adequate volume of Laemmli buffer.

Approximately 20 μg of proteins per sample were separated by electrophoresis on 12% TGX Stain-Free FastCast polyacrylamide gels (Bio-Rad, Hercules, CA). An unstained protein standard (Bio-Rad) was used for molecular weight determination. Electrophoresis was conducted at 200 V for 35 min in a TGS buffer (25 mM Tris, 192 mM glycine, 0.1% SDS). Protein bands were visualized using ChemiDoc MP (Bio-Rad) with Stain-Free activation (UV exposure, 45 s) without staining. Proteins

were transferred to nitrocellulose membranes using the Trans-Blot Turbo system (Bio-Rad) at 1.3 A, 25 V for 5 min. Membranes were blocked with EveryBlot Blocking Buffer (Bio-Rad) for 5 min and washed twice with TBS 1X containing 0.1% Tween-20. Primary antibodies (anti-ZEP - zeaxanthin epoxidase, AS234947; Agrisera AB, Vännäs, Sweden) were diluted 1:3000 in the blocking buffer and incubated for 1 h with gentle rocking. Following washes, membranes were incubated with goat anti-rabbit IgG StarBright Blue 700 secondary antibody (Bio-Rad, diluted 1:2500) for 1 h. Protein transfer efficiency was verified by Stain-Free blot imaging. Band intensities were quantified using Bio-Rad Image Lab software and normalized to a reference lane on each membrane. Results are presented as the variation of the stressed group relative to its control group, calculated as [(stressed group – control group)/control group] x 100.

2.8. Statistical analysis

For each genotype, the distribution of data within each treatment was tested for normality using the Shapiro-Wilk normality test. The differences between the experimental groups in Tables 2 and 3 were assessed by a two-way ANOVA followed by a Tukey's post hoc test. A two-way ANOVA followed by a Tukey's post hoc test was performed on the ABA test (Fig. 5). The *t*-test was used to assess the physiological differences between the control and stress samples at the day level (Figs. 1–3) and on the heatmap (Fig. 4). These data analyses and graphs were carried out using the latest stable release of RStudio, version 4.4.1 (Posit PBC, Boston, USA).

3. Results

3.1. Water deficit and salinity cause similar physiological behaviour in leaves, but differ in their dependence on genotype

We assessed the variability in the response of physiological and biometric traits to water deficit and salt treatments conditions using analysis of variance (ANOVA). We reported the statistical significance of the main factors (genotype and treatment) and their interaction (see Tables 2 and 3).

Physiological analyses of gas exchange and photosynthetic performance revealed pronounced stress-induced alterations. Both water deficit and salinity treatments significantly decreased stomatal conductance (gsw; $p < 0.001$). A genotype effect was detected only in the water deficit experiment (DS). However, the lack of a significant genotype × treatment interaction indicated that the genotypes did not differ in the magnitude of their gsw responses. Net CO_2 assimilation (A) was significantly influenced by genotype, treatment, and their interaction under both stress conditions. Although the G × S interaction was not significant, water-use efficiency (WUE) was significantly affected by treatment in both experiments (Supplementary Material, Fig. S2). In a scenario of drought stress, the effective quantum yield of PSII and the electron transport rate were strongly influenced by genotype, treatment, and the interaction between the two. Under salt stress, however, ΦPSII and ETR (Supplementary Material, Fig. S3) were affected only by genotype and the G × S interaction, rather than the treatment. Under water deficit, Dog Ridge exhibited the highest ΦPSII and ETR, whereas Kober 5BB and M2 showed the lowest values. By contrast, Kober 5BB displayed higher photochemical performance during salinity exposure, while M4

Table 2
The effects of factors "genotype" (G), "treatment" (S), and their interaction (G × S), as well as their statistical significance, on the following parameters at the end of water deficit treatment (DS): stomatal conductance (gsw), net CO_2 assimilation (A), water use efficiency (WUE), quantum yield of photosystem II (ΦPSII), electron transport rate (ETR) and the maximum quantum efficiency of PSII (Fv/Fm), fresh weight of leaves and roots (FW), dry weight of leaves and roots (DW) and water content of leaves and roots (WC). Each value represents the mean ± standard deviation. Asterisks indicate levels of statistical significance: * p-value < 0.05, ** p-value < 0.01, *** p-value< 0.001.

Physiological Data						
DS	gsw	A	WUE	ΦPSII	ETR	Fv/Fm
Genotype (G)						
140 Ruggeri	0.06 ± 0.04 ab	3.45 ± 1.89 abc	67.90 ± 15.11 ab	0.02 ± 0.01 ab	20.68 ± 10.41 ab	0.79 ± 0.06
Dog Ridge	0.07 ± 0.03 a	4.13 ± 1.04 a	64.82 ± 14.98 ab	0.03 ± 0.01 a	27.00 ± 4.87 a	0.87 ± 0.03
Kober 5BB	0.05 ± 0.04 b	2.92 ± 1.79 bc	70.82 ± 18.04 a	0.02 ± 0.01 b	17.58 ± 6.53 b	0.83 ± 0.04
M2	0.05 ± 0.03 b	2.56 ± 1.12 c	62.87 ± 15.42 ab	0.02 ± 0.00 b	17.48 ± 2.37 b	0.84 ± 0.06
M4	0.08 ± 0.03 a	3.84 ± 1.26 ab	55.35 ± 12.52 b	0.02 ± 0.00 ab	20.15 ± 2.10 ab	0.85 ± 0.07
p-value	**<0.001** ***	**<0.001** ***	**0.037** *	**0.003** **	**0.003** **	**0.103**
Treatment (S)						
CTRL t1	0.09 ± 0.02 a	4.58 ± 0.70 a	52.23 ± 6.63 b	0.03 ± 0.01 a	23.37 ± 6.13 a	0.86 ± 0.04 a
DS t1	0.03 ± 0.02 b	2.17 ± 0.97 b	76.47 ± 10.91 a	0.02 ± 0.01 b	17.78 ± 6.11 b	0.81 ± 0.06 b
p-value	**<0.001** ***	**<0.001** ***	**<0.001** ***	**0.001** **	**0.001** **	**0.006** **
G x S						
p-value	**0.158**	**0.020** *	**0.7301**	**0.003** **	**0.003** **	**0.432**
Biometric Data						
DS	FW leaves	DW leaves	WC leaves	FW roots	DW roots	WC roots
Genotype (G)						
140 Ruggeri	3.45 ± 1.02 a	0.76 ± 0.17 a	3.56 ± 0.75	2.76 ± 1.47	0.21 ± 0.07	11.69 ± 3.52
Dog Ridge	1.82 ± 0.73 b	0.35 ± 0.13 c	4.24 ± 0.70	2.78 ± 1.21	0.21 ± 0.05	13.05 ± 6.40
Kober 5BB	2.94 ± 1.25 a	0.63 ± 0.14 ab	3.57 ± 1.60	2.72 ± 1.07	0.20 ± 0.05	12.33 ± 4.36
M2	2.58 ± 1.00 ab	0.52 ± 0.18 bc	3.98 ± 0.76	2.05 ± 0.86	0.15 ± 0.04	12.15 ± 3.54
M4	2.45 ± 1.05 ab	0.60 ± 0.23 ab	3.38 ± 1.74	2.03 ± 0.86	0.14 ± 0.04	13.13 ± 3.63
p-value	**0.003** **	**<0.001** ***	**0.463**	**0.134**	**0.050**	**0.758**
Treatment (S)						
CTRL t1	3.15 ± 1.19 a	0.61 ± 0.25	4.29 ± 0.80 a	3.16 ± 1.06 a	0.19 ± 0.06	15.78 ± 2.04 a
DS t1	2.14 ± 0.76 b	0.53 ± 0.16	3.21 ± 1.27 b	1.78 ± 0.65 b	0.18 ± 0.05	9.16 ± 3.10 b
p-value	**<0.001** ***	**0.126**	**0.002** **	**<0.001** ***	**0.493**	**<0.001** ***
G x S						
p-value	**0.010** *	**0.114**	**0.229**	**0.110**	**0.074**	**0.087**

Table 3
The effects of factors "genotype" (G), "treatment" (S), and their interaction (G × S), as well as their statistical significance, on the following parameters at the end of salt stress: stomatal conductance (gsw), net CO_2 assimilation (A), water use efficiency (WUE), quantum yield of photosystem II (ΦPSII), electron transport rate (ETR) and the maximum quantum efficiency of PSII (Fv/Fm), fresh weight of leaves and roots (FW), dry weight of leaves and roots (DW) and water content of leaves and roots (WC). Each value represents the mean ± standard deviation. Asterisks indicate levels of statistical significance: * p-value < 0.05, ** p-value < 0.01, *** p-value< 0.001.

Physiological Data						
SS	gsw	A	WUE	ΦPSII	ETR	Fv/Fm
Genotype (G)						
140 Ruggeri	0.07 ± 0.01	3.69 ± 0.58 ab	52.93 ± 7.08	0.02 ± 0.00 bc	18.98 ± 3.37 bc	0.90 ± 0.06
Dog Ridge	0.07 ± 0.02	3.76 ± 1.10 a	57.60 ± 5.24	0.03 ± 0.01 ab	23.61 ± 5.79 ab	0.86 ± 0.04
Kober 5BB	0.07 ± 0.03	3.94 ± 1.17 a	56.89 ± 9.31	0.03 ± 0.01 a	27.19 ± 6.98 a	0.88 ± 0.04
M2	0.06 ± 0.02	3.27 ± 0.39 ab	56.49 ± 15.98	0.02 ± 0.01 ab	20.53 ± 9.30 ab	0.83 ± 0.07
M4	0.06 ± 0.03	3.03 ± 0.83 b	53.77 ± 18.13	0.02 ± 0.00 c	13.07 ± 3.08 c	0.87 ± 0.05
p-value	**0.606**	**0.006** **	**0.917**	**<0.001** ***	**<0.001** ***	**0.153**
Treatment (S)						
CTRL t1	0.08 ± 0.02 a	4.13 ± 0.79 a	50.27 ± 8.20 b	0.03 ± 0.01	21.85 ± 8.42	0.89 ± 0.06 a
SS t1	0.05 ± 0.01 b	2.95 ± 0.47 b	60.80 ± 12.16 a	0.02 ± 0.01	19.50 ± 6.47	0.84 ± 0.04 b
p-value	**<0.001** ***	**<0.001** ***	**0.012** *	**0.124**	**0.124**	**0.010** *
G x S						
p-value	**0.096**	**0.001** **	**0.203**	**<0.001** ***	**<0.001** ***	**0.502**
Biometric Data						
SS	FW leaves	DW leaves	WC leaves	FW roots	DW roots	WC roots
Genotype (G)						
140 Ruggeri	5.78 ± 1.55 b	1.25 ± 0.42 bc	3.71 ± 0.45 b	5.93 ± 2.45 b	0.45 ± 0.18 c	12.02 ± 0.67 a
Dog Ridge	5.44 ± 1.10 b	1.16 ± 0.14 bc	3.68 ± 0.71 b	8.17 ± 1.52 b	0.66 ± 0.20 b	11.87 ± 1.91 a
Kober 5BB	7.39 ± 3.70 a	1.42 ± 0.78 ab	4.35 ± 0.41 a	6.61 ± 3.48 a	0.63 ± 0.38 b	10.12 ± 1.76 bc
M2	5.27 ± 0.88 b	1.09 ± 0.19 c	3.83 ± 0.19 b	6.34 ± 0.95 b	0.55 ± 0.09 bc	10.64 ± 0.61 b
M4	8.22 ± 2.06 a	1.59 ± 0.51 a	4.30 ± 0.46 a	8.83 ± 3.20 a	0.90 ± 0.44 a	9.40 ± 1.49 c
p-value	**<0.001** ***	**<0.001** ***	**<0.001** ***	**<0.001** ***	**<0.001** ***	**<0.001** ***
Treatment (S)						
CTRL t1	5.33 ± 1.32 b	1.01 ± 0.25 b	4.30 ± 0.37 a	5.21 ± 1.63 b	0.41 ± 0.12 b	11.67 ± 1.42 a
SS t1	7.51 ± 2.62 a	1.60 ± 0.48 a	3.65 ± 0.48 b	9.13 ± 1.89 a	0.86 ± 0.28 a	9.95 ± 1.48 b
p-value	**<0.001** ***	**<0.001** ***	**<0.001** ***	**<0.001** ***	**<0.001** ***	**<0.001** ***
G x S						
p-value	**<0.001** ***	**<0.001** ***	**0.033** *	**<0.001** ***	**<0.001** ***	**<0.001** ***

exhibited the least efficient response. The maximum quantum efficiency of PSII (Fv/Fm) was significantly affected only by treatment (Supplementary Material, Fig. S4).

Tables 2 and 3 report biometric traits, including fresh weight (FW), dry weight (DW) and water content (WC) of leaves and roots. The grapevine genotypes showed distinct functional strategies in how they regulated tissue hydration, and growth under water deficit and salt conditions. During the water deficit, the 140 Ruggeri and Dog Ridge rootstocks adopted a conservative strategy, maintaining structural biomass (DW was not statistically significantly influenced by the treatment), while mainly modulating water status; leaf FW and DW differed between genotypes, with 140 Ruggeri showing the highest values and Dog Ridge the lowest, but FW declined across all genotypes and DW remained stable, indicating that dehydration rather than growth inhibition dominated the response; genotype × treatment effects were limited to leaf FW. Under salinity, responses were more plastic and genotype-dependent, involving adjustments in hydration and growth. Kober 5BB, 140 Ruggeri and M4 increased FW and DW in both leaves and roots despite not changing or reducing the WC (Table S4), indicating active biomass accumulation and possible osmotic adjustment; Kober 5BB showed the highest leaf FW and WC, whereas M4 accumulated the greatest leaf DW and the largest root biomass, although with the lowest root WC, consistent with investment in root growth under osmotic stress. M2 showed the lowest leaf FW and DW, reflecting limited growth capacity and a more conservative strategy. 140 Ruggeri, despite having the lowest root biomass, maintained the highest root WC, suggesting higher water-retention efficiency. Overall, drought primarily elicited water-loss–driven adjustments with stable structural biomass, whereas salinity triggered growth remodelling and biomass accumulation despite reduced WC, pointing to distinct mechanistic bases for stress tolerance in these genotypes.

Physiological traits can be described by grouping genotypes based on their physiological behaviour. Genotypes with a stable or low-sensitivity response to stress were 140 Ruggeri, Kober 5BB and M2. These three genotypes exhibited relatively conservative behaviour, with reductions in gsw that only emerged in the final stages of stress or were modest overall. Under water deficit conditions (Figs. 1A), 140 Ruggeri maintained a stable trend, with significant declines only at the end of the treatment. Under salinity (Fig. 1B), it did not show a progressive decline and the values remained similar to the control. Kober 5BB exhibited a similar pattern: there was no significant reduction during the water deficit, except for a final decline (Fig. 1E). Under salinity, gsw remained consistent with the control group (Fig. 1F). M2 was the most stable. Under water deficit, gsw did not differ from the control until the final sampling point (Fig. 1G). Under salinity, no significant differences were observed throughout the entire treatment period (Fig. 1H). Dog Ridge is an example of genotypes with a differentiated response depending on stress. Dog Ridge exhibited a response similar to stable genotypes under water deficit conditions but behaved very differently under salinity conditions. Under water deficit conditions, the reduction in gsw only occurred towards the end, in a manner similar to that observed for 140 Ruggeri (Fig. 1C). However, under salinity, it exhibited an early and marked decline of 56% compared to t0, with values significantly lower than the control for most of the treatment period (Fig. 1D). M4 exemplified genotypes that were sensitive to both stresses. M4 was the most responsive genotype, showing early and persistent reductions. Under water deficit conditions, decreases in gsw were evident by day 12 (Fig. 1I). Under salinity conditions, gsw was consistently lower than in

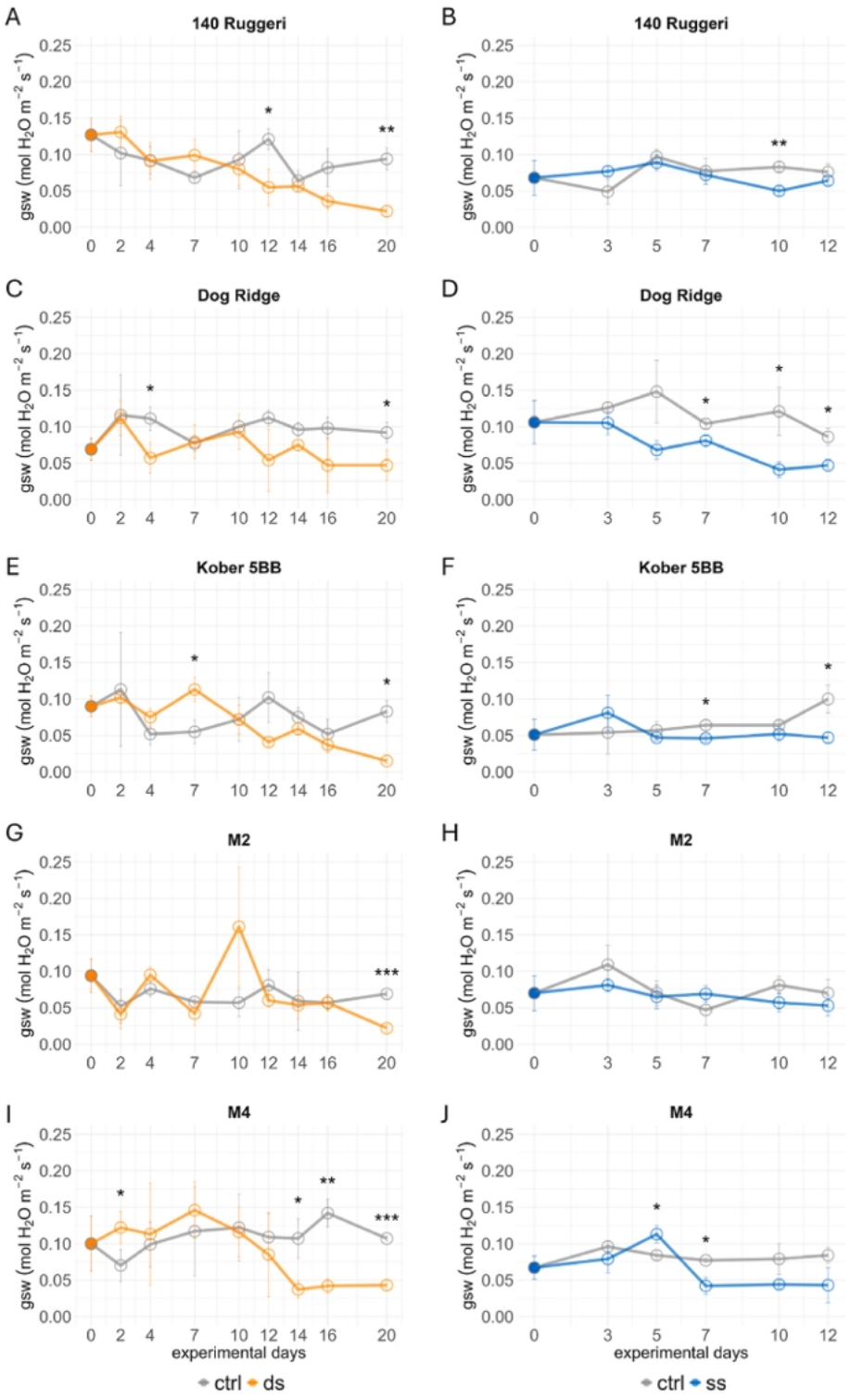

Fig. 1. Stomatal conductance (gsw) in control (grey) and drought-stressed (orange) grapevine genotypes from day 0 to day 20 (A, C, E, G, I) and in control (grey) and salt-stressed (blue) grapevine genotypes from day 0 to day 12 (B, D, F, H, J). At day 0 the stressed and control samples were still one group. Within each time point, statistical significance between control and stressed samples was determined by Student's t-test (*** p-value < 0.001; ** p-value < 0.01; * p-value < 0.05).

the control group, although the reduction was less pronounced (Fig. 1J).

Genotypes could also be grouped according to their behaviour in terms of CO_2 assimilation. The M2 and Kober 5BB genotypes remained stable under conditions of both drought and salt stress. Throughout the water deficit period, M2 maintained A values comparable to those of the control group, experiencing a decline only on the final day (Fig. 2G). Salinity remained remarkably stable, with values close to those of the control group and only slight significant differences (Fig. 2H). Under water deficit conditions, Kober 5BB exhibited unusual behaviour in the early days, initially increasing in A before returning to control levels (Fig. 2E). Under salinity conditions, A remained slightly lower than the control group throughout the treatment period (Fig. 2F). Conversely, the 140 Ruggeri and M4 genotypes were sensitive to both drought and salt stress. Ruggeri exhibited a constant but low reduction in net CO_2

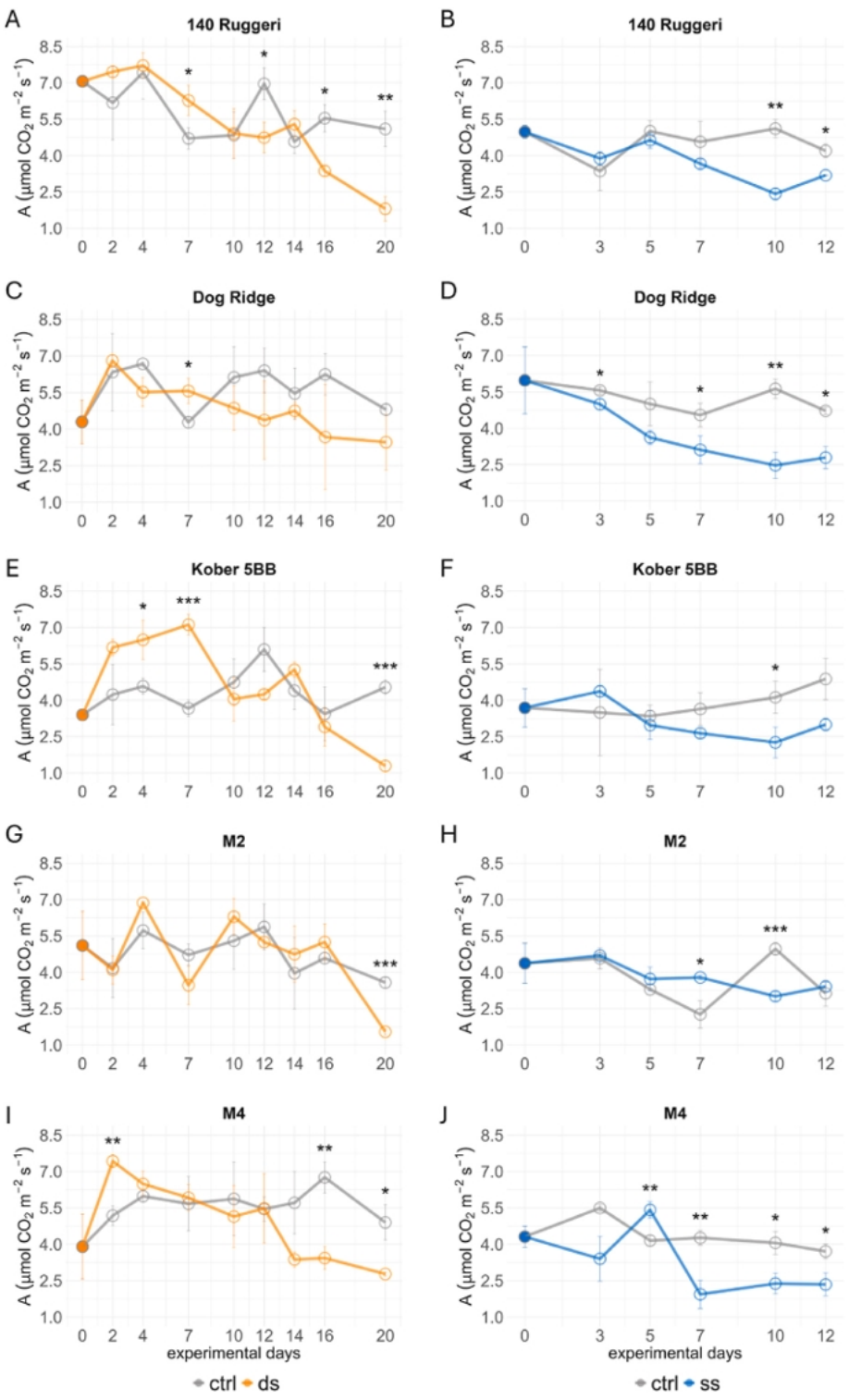

Fig. 2. Net CO_2 assimilation in control (grey) and drought-stressed (orange) grapevine genotypes from day 0 to day 20 (A, C, E, G, I) and in control (grey) and salt-stressed (blue) grapevine genotypes from day 0 to day 12 (B, D, F, H, J). At day 0 the stressed and control samples were still one group. Within each time point, statistical significance between control and stressed samples was determined by Student's t-test (*** p-value < 0.001; ** p-value < 0.01; * p-value < 0.05).

assimilation during water deficit. However, the reduction was sharper during the first few days of the experiment (Fig. 2A). A similar trend was observed under salinity conditions, but the reduction was more moderate (−24%) and limited to the final stages (see Fig. 2B). M4 exhibited a similar trend under water deficit and salt stress conditions (see Fig. 2I and J). A values declined significantly and suddenly in the final days of both experiments. In conclusion, both the 140 Ruggeri and the M4 were sensitive to stress, but there were some significant differences between them. The Dog Ridge genotype exhibited a differentiated response depending on stress. Dog Ridge exhibited a moderate and delayed response to drought, but an early and pronounced sensitivity to salinity. Under water deficit conditions, there were no statistically significant changes in A, but the mean values remained consistently lower than those of the control (see Fig. 2C). Under salinity, the reduction was rapid

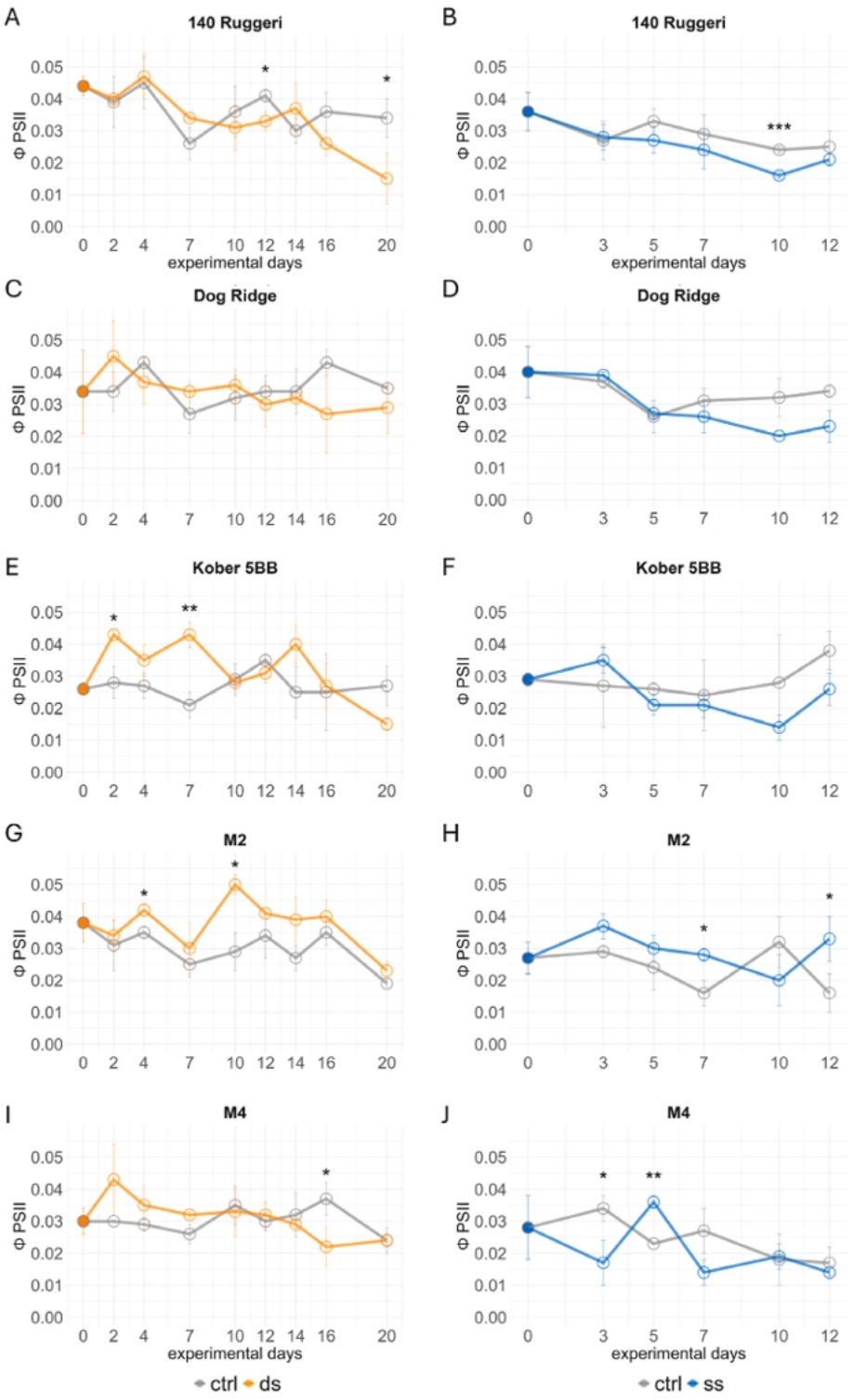

Fig. 3. Quantum yield of photosystem II (ΦPSII), in control (grey) and drought-stressed (orange) grapevine genotypes from day 0 to day 20 (A, C, E, G, I) and in control (grey) and salt-stressed (blue) grapevine genotypes from day 0 to day 12 (B, D, F, H, J). At day 0 the stressed and control samples were still one group. Within each time point, statistical significance between control and stressed samples was determined by Student's t-test (*** p-value < 0.001; ** p-value < 0.01; * p-value < 0.05).

and substantial; after just three days, it had fallen by 40% (Fig. 2D).

The analysis of PSII photochemical behaviour allowed the identification of distinct response groups. The 140 Ruggeri and Dog Ridge genotypes exhibited stable PSII photochemistry in response to both stresses. These genotypes showed a marked stability of PSII photochemistry, with minimal variations generally limited to single sampling points. 140 Ruggeri maintained ΦPSII values comparable to the control during water deficit, except for the final significant decline (Fig. 3A), and under salinity, where only one point differed from the control (Fig. 3B). Dog Ridge displayed an even stronger stability eith ΦPSII varying little and not showing substantial deviations under either water deficit or salinity (Fig. 3C and D). The genotypes with transient or non-

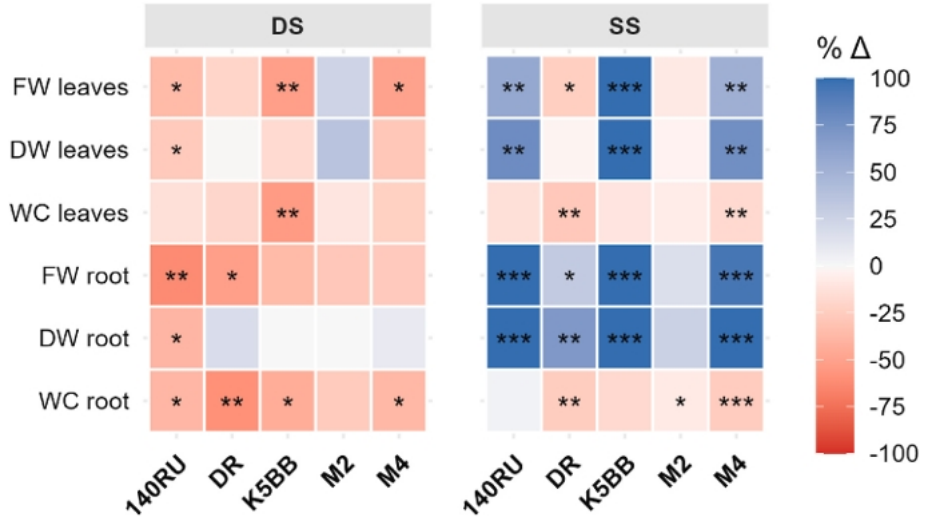

Fig. 4. Heat map of the percentage variation (%Δ) in biometric parameters on the differences between drought-stressed (DS) and salt-stressed (SS) samples compared to their respective controls, on the last day of the experiment, for five grapevine rootstocks (140 Ruggeri, Dog Ridge, Kober 5BB, M2, and M4). Color intensity represents the magnitude of change; asterisks indicate levels of statistical significance: * p-value < 0.05, ** p-value < 0.01, *** p-value< 0.001.

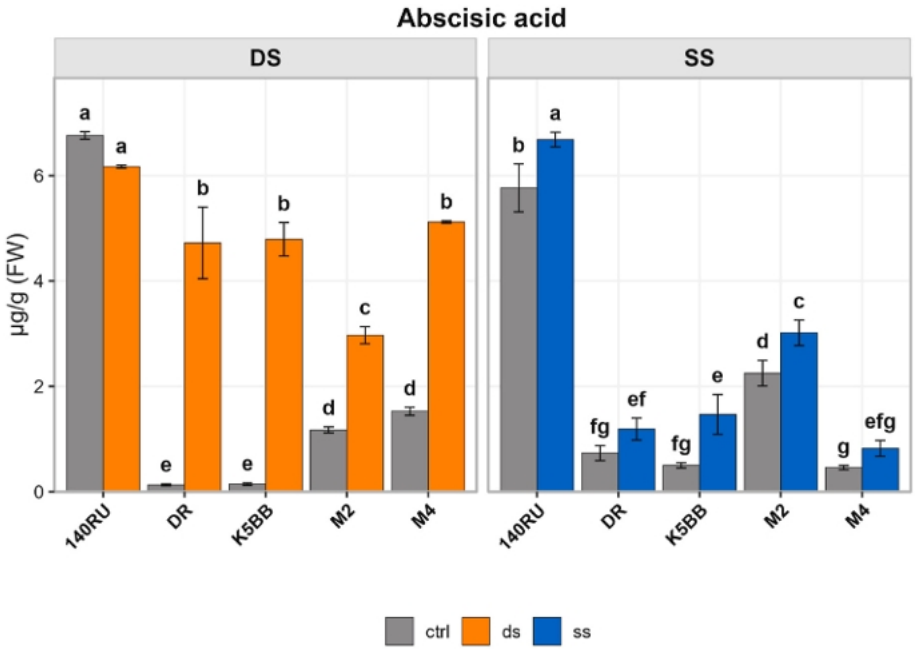

Fig. 5. ABA (abscisic acid) content of five different grapevine rootstock genotypes (140 Ruggeri, Dog Ridge, Kober 5BB, M2 and M4) under drought and salt stress. The bar plots show the mean ABA content (µg/g FW) under control conditions (grey), in response to drought stress (orange), and in response to salt stress (blue). Vertical bars represent the standard deviation of the mean. Different letters above the bars indicate statistically significant differences in means according to Tukey's HSD post hoc test (p-value < 0.05), which was performed separately for the DS and SS experimental sets.

linear responses were Kober 5BB, M2 and M4. These genotypes showed temporary oscillations in ΦPSII, without persistent deviations from the control. Kober 5BB under water deficit exhibited an early increase in ΦPSII, followed by a gradual return to control levels (Fig. 3E). Under salinity, ΦPSII remained essentially unchanged compared with the control (Fig. 3F). M2 showed an intermediate peak of ΦPSII during water deficit treatment (Fig. 3G), while under salinity it maintained values very close to the control for most of the treatment (Fig. 3H). M4 displayed a pattern similar to M2: under water deficit only one sampling point differed from the control (Fig. 3I), whereas under salinity only a transient fluctuation occurred midway through the treatment (Fig. 3J). For all genotypes, the trend of ETR mirrored that of ΦPSII, with no substantial divergence between the two parameters under either stress condition (Supplementary Material, Fig. S3).

To analyse the biometric parameters, we chose to present the percentage variation (Δ%) in the form of a heat map to determine the difference between the samples subjected to water deficit and salt stress and their respective controls on the last day of the analysis (Fig. 4). The raw data underlying the heatmap are provided in Supplemental Tables S3 and S4. Under water deficit conditions, the genotypes 140 Ruggeri, Kober 5BB, and M4 exhibited reductions in leaf fresh weight (FW). However, only 140 Ruggeri showed a concomitant decrease in leaf dry weight (DW), whereas the reductions observed in the other genotypes were attributable primarily to loss of water content (WC). In roots, both 140 Ruggeri and Dog Ridge showed decreased FW under water deficit, but only 140 Ruggeri also exhibited a decline in DW. No

reductions in root DW were detected in the remaining genotypes, which instead showed decreases in WC, with the exception of M2. Notably, M2 was the only genotype to display an increase in both leaf FW and DW under water deficit, although these changes were not statistically significant. Under salinity, leaf FW and DW increased in 140 Ruggeri, Kober 5BB, and M4. In M4, the rise in leaf DW was statistically significant, leading to higher FW despite reduced WC. Dog Ridge was the only genotype to show a reduction in leaf FW under salinity, corresponding to a loss in WC. In contrast, M2 showed leaf biomass patterns similar to the control. For roots, all genotypes increased both FW and DW under salinity except M2, whose root biomass remained unchanged. Root WC decreased in Dog Ridge, M2, and M4.

3.2. Drought-associated ABA accumulation is stronger than salt-induced ABA production and contributes to stomatal regulation

An analysis of abscisic acid (ABA) levels under control, water deficit and salinity conditions was performed to test whether tolerance to stress was associated with hormonal changes (Fig. 5). The genotype 140 Ruggeri consistently exhibited high basal ABA concentrations in both experiments, and ABA levels remained elevated in both control and stressed plants. Under salinity, a slight but detectable increase in ABA was observed relative to the control. Dog Ridge showed an approximately fivefold increase in ABA under water deficit, a response that paralleled the marked decline in stomatal conductance. In contrast, no increase in ABA was detected under salt stress. Kober 5BB displayed a similar pattern: ABA levels rose roughly fivefold under water deficit, whereas under salinity ABA content doubled relative to the control, a difference that was statistically significant but substantially less pronounced than under water deficit. In genotype M2, ABA levels increased significantly under both water deficit and salinity, although the drought-induced accumulation was markedly stronger than the response to salt stress. M4 showed a roughly threefold increase in ABA under water deficit, whereas no significant changes were observed under salinity. Overall, Dog Ridge, Kober 5BB, M2, and M4 showed consistent ABA accumulation in stressed plants, reflecting a robust hormonal response to water deficit. Under salinity, ABA induction was generally weaker or absent, with the notable exception of 140 Ruggeri, which maintained high ABA levels under both control and stress conditions and showed only a modest increase under salt exposure.

3.3. ZEP immunoreactivity reveals that stress-specific regulation only partially tracks ABA accumulation

In order to test whether stress-dependent ABA content was accompanied by the differential regulation of ABA biosynthetic machinery, we analysed the immunoreactivity of ZEP in leaves and roots. ZEP (zeaxanthin epoxidase) plays a pivotal role in the initial stage of ABA biosynthesis. Acting within the carotenoid branch of the pathway, ZEP catalyses the conversion of zeaxanthin to violaxanthin, providing essential precursors for ABA synthesis. Immunoblotting using an anti-ZEP antibody revealed two main immunoreactive bands, measuring

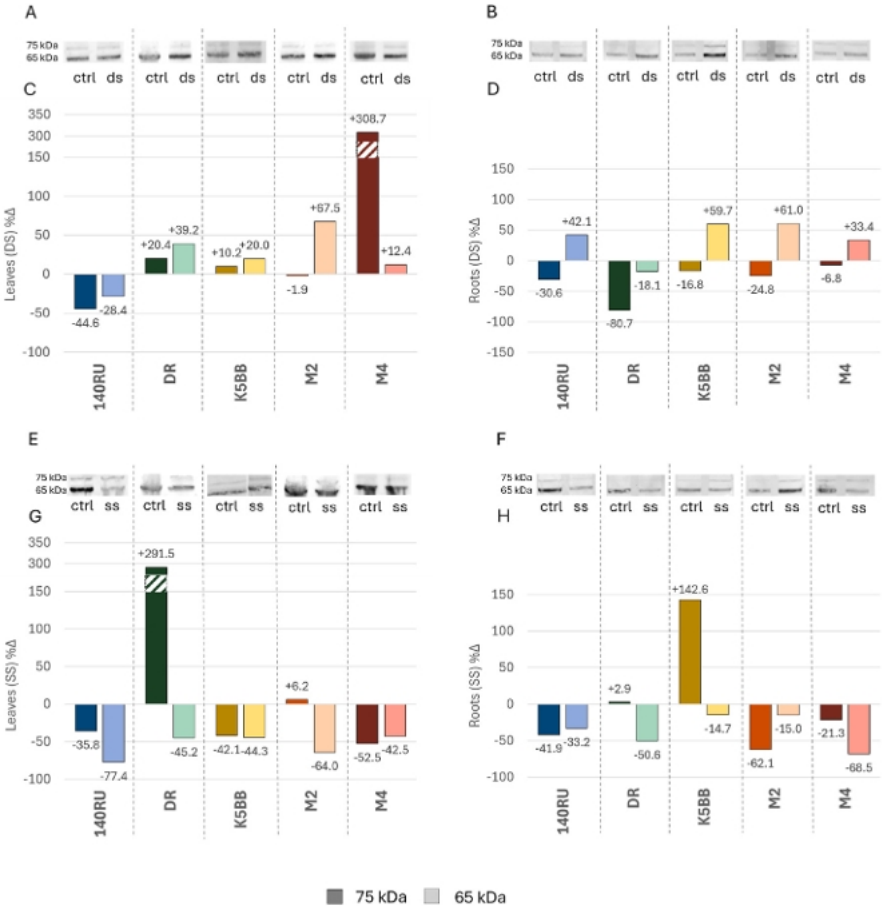

Fig. 6. ZEP immunoblot analysis in grapevine leaves and roots under drought and salt stress. Representative immunoblots (top of each panel) show anti-ZEP immunoreactive bands at ~75 kDa and ~65 kDa in protein extracts from leaves (A, E) and roots (B, F) of five grapevine genotypes (140RU, K5BB, DR, M2, M4) grown under control conditions (ctrl) or exposed to drought stress (DS; A–D) or salt stress (SS; E–H). Densitometric quantification is reported below each blot as percent change relative to the corresponding control (C, D, G, H). In the bar plots, the ~65 kDa band is represented by light color bars and the ~75 kDa band by dark color bars.

approximately 75 and 65 kDa (kDa), in the leaves and roots of the five grapevine genotypes subjected to water deficit (DS) and salt stress (SS) (Fig. 6). Densitometric values are reported as a percentage of the corresponding control. In the leaves (see Fig. 6A and C), the DS treatment resulted in genotype-dependent changes to the 75-kDa signal. These changes ranged from a 45% decrease in 140RU to modest increases of 10% in K5BB and 20% in DR, and a strong 309% increase in M4. There was also near-stability in M2. Analysis of the 65-kDa band in the leaves (see Fig. 6A and C) showed an increase in most genotypes exposed to DS (from +12% in M4 to +68% in M2). The exception was the 140RU genotype, for which a 28% decrease was observed. In the root samples (see Fig. 6B and D), the same treatment resulted in a general decrease in the 75-kDa band across all genotypes, including 140RU (−31%), DR (−81%), K5BB (−17%), M2 (−25%) and M4 (−7%). Conversely, the 65-kDa band increased in the 140RU, K5BB, M2 and M4 genotypes (+42%, +60%, +61% and +33% respectively), while it decreased in the DR genotype (−18%). Under SS conditions, the pattern in the leaves (see Fig. 6E and G) was more consistent, with a decrease in the 65-kDa band observed across all genotypes. Reductions ranged from 43% (M4) to 77% (140RU). The response of the 75 kDa band, however, was more heterogeneous: a decrease was observed in 140RU, K5BB, and M4, a slight increase in M2, and a strong induction in the DR genotype. In the roots (Fig. 6F and H), SS again caused a reduction in the 65 kDa signal in all genotypes, with intensities ranging from −15% (K5BB and M2) to −68% (M4). The 75 kDa response in roots was genotype-specific, with a significant increase in K5BB (+143%), minimal change in DR (+3%),

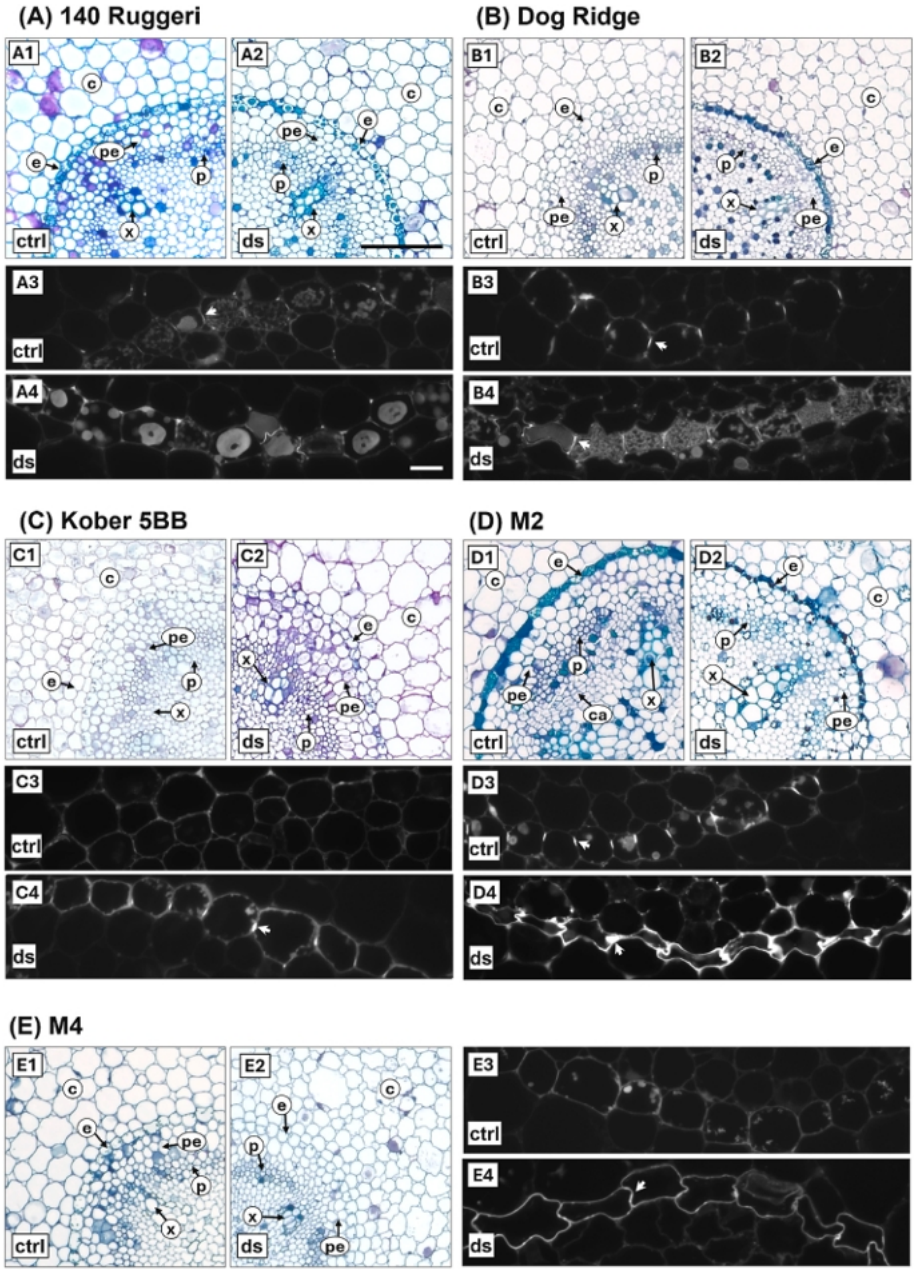

Fig. 7. Root cross-sections of five different rootstocks at timepoint 1: A) 140 Ruggeri, B) Dog Ridge, C) Kober 5BB, D) M2; and E) M4. Micrographs 1 and 2 show, respectively, control samples (t1) and drought-stressed samples stained with Toluidine Blue O (TBO). Micrographs 3 and 4 show, respectively, control samples (T1) and drought-stressed samples stained with Fluorol Yellow 088. The labels indicate the following key anatomical structures: c = cortex; e = endodermis; p = phloem vessel; pe = pericycle; x = xylem vessel; ca = cambium; arrows show suberin lamellae. The scale bar in Micrograph A2 represents 100 μm and applies to all micrographs 1 and 2 in the figure. The scale bar in Micrograph A4 represents 10 μm and applies to all micrographs 3 and 4 in the figure.

and consistent reductions in 140RU (−42%), M2 (−62%), and M4 (−21%). Overall, salt stress uniformly suppressed the 65 kDa ZEP signal in both organs, while water deficit tended to increase the 65 kDa signal and decrease the 75 kDa signal in roots. The 75 kDa band exhibited the most pronounced genotype-specific induction in M4 (leaves, DS), DR (leaves, SS) and K5BB (roots, SS). In general, ZEP immunoreactivity changed in a manner dependent on stress, organ and genotype. However, it did not uniformly mirror ABA accumulation, which suggests the presence of additional regulatory levels.

3.4. Root endodermal remodelling differentiates rootstock strategies in response to water deficit and salinity

The histological analysis of roots aimed to identify morphological features explaining differences in stress tolerance. In Figs. 7 and 8, micrographs with suffix "1" and "2" show TBO-stained root histology; micrographs with the suffixes "3" and "4" show suberin lamellae stained with Fluorescein Yellow 088 (FY) in the endodermis of control and water-deprived or salt-stressed plants.

*Water deficit treatment*In the 140 Ruggeri genotype (Fig. 7A1-2), root organisation (including cortex (c), endodermis (e), pericycle (pe) and differentiated phloem (p) and xylem (x)) was preserved under both conditions. Under control conditions (Fig. 7A1), cortical cells were large and turgid, with a continuous endodermis and a regular pericycle, xylem and peripheral phloem. Under water-restricted conditions (Fig. 7A2), cortical cells were less turgid and irregular, reflecting reduced water availability. Endodermis and pericycle were unchanged, but phloem continuity and xylem development decreased. These anatomical

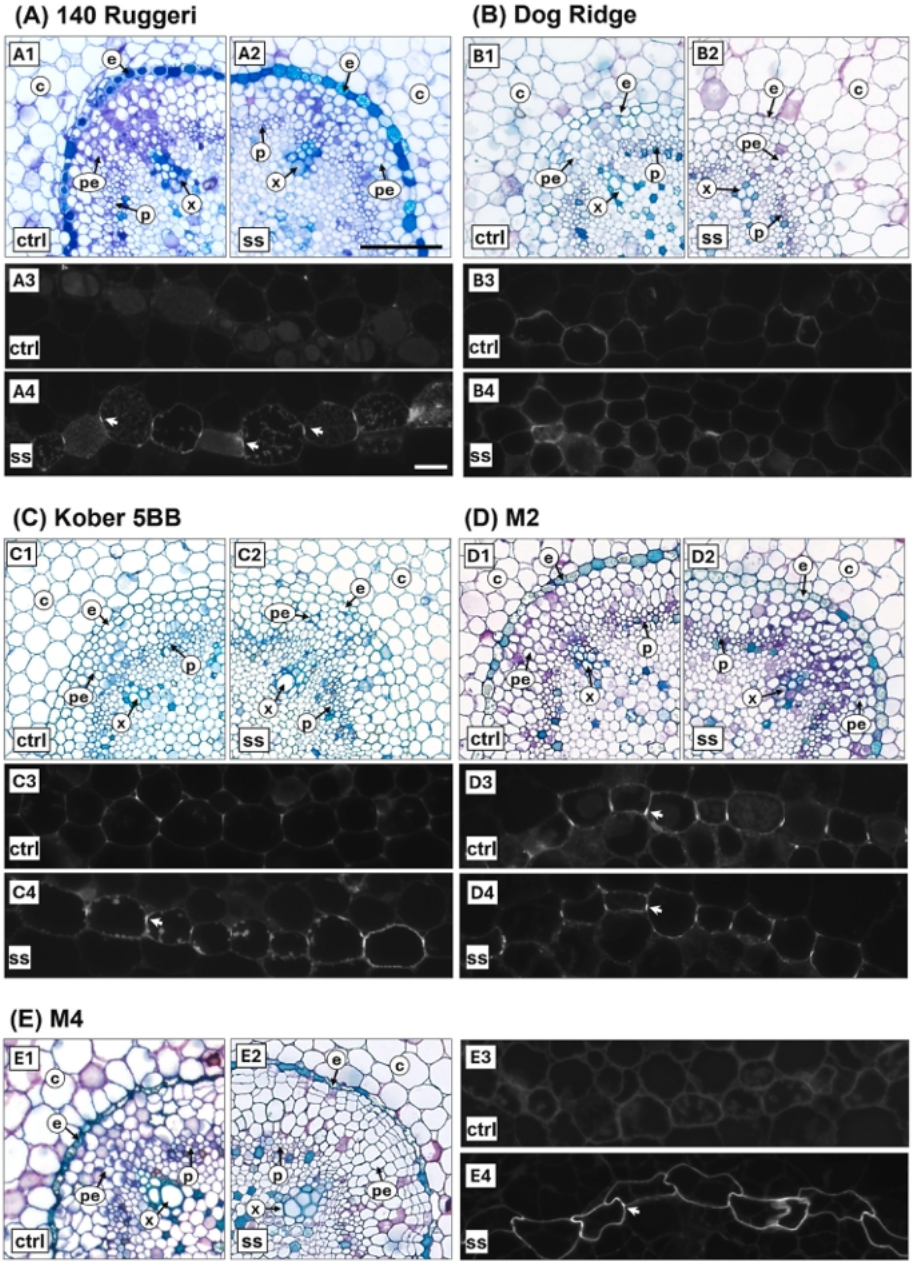

Fig. 8. Root cross-sections of five different rootstocks at timepoint 1: A) 140 Ruggeri, B) Dog Ridge, C) Kober 5BB, D) M2; and E) M4. Micrographs 1 and 2 show, respectively, control samples (t1) and salt-stressed samples stained with Toluidine Blue O (TBO). Micrographs 3 and 4 show, respectively, control samples (t1) and salt-stressed samples stained with Fluorol Yellow 088. The labels indicate the following key anatomical structures: c = cortex; e = endodermis; p = phloem vessel; pe = pericycle; x = xylem vessel; ca = cambium; arrows show suberin lamellae. The scale bar in Micrograph A2 represents 100 μm and applies to all micrographs 1 and 2 in the figure. The scale bar in Micrograph A4 represents 10 μm and applies to all micrographs 3 and 4 in the figure.

changes indicate cortical and vascular adjustments associated with water deficit. Fig. 7A3 and 7A4 show that genotype 140 Ruggeri exhibited a weak FY signal under both conditions, with minimal suberin accumulation between adjacent cells (arrows). This suggests that water-limiting treatment did not improve endodermis suberisation.

In Dog Ridge (Fig. 7B1-2), root anatomy remained intact under both control (B1) and water-limiting (B2) conditions, though the A_{stele}-to-A_{total} ratio increased under water-limiting conditions (Table S5). Control roots had large, hydrated cortical cells. The endodermis was less identifiable, while pericycle and vascular tissues (with central xylem and peripheral phloem) were more distinct. Under water deficit conditions, cortical cells appeared less turgid and more compact, the endodermis became more pronounced and intensely stained, suggesting an enhanced barrier function. The pericycle also showed structural modifications. Phloem continuity and xylem development declined. These changes indicate water deprivation-related reorganisation of cortical, endodermal, pericyclic and vascular tissues in Dog Ridge roots. In control samples, suberin lamellae in Dog Ridge appeared as small thin structures between adjacent cells (see arrow in Fig. 7B3). Water-limiting stress, however, increased suberisation of the endodermis cell wall in Dog Ridge, forming continuous, more compact strips connecting adjacent cells (see arrows in Fig. 7B4).

In Kober 5BB (Fig. 7C1-2), cortical cells were well expanded and regularly arranged under control conditions (C1), while the endodermis was barely visible. The pericycle was organised, with distinct phloem and poorly developed xylem, and appeared thicker under water-limiting conditions (Table S5). Under water deficit (C2), organisation of cortical cells was largely unchanged, but cells were irregular and the cortex area increased, as shown by higher cortex/total ratio and lower stele/total ratio (Table S5). By contrast, the endodermis became more evident and compact, suggesting enhanced control of radial water flow. Meanwhile, phloem appeared less distinct, and xylem development was more advanced than in control. Overall, water deprivation primarily affected endodermis and vascular tissues, indicating adaptive anatomical adjustments to limited water availability. Water deprivation also improved suberin lamella formation in Kober 5BB. Under control (Fig. 7C3), FY-stained suberin lamellae were absent, whereas under water restriction (Fig. 7C4), endodermis cells showed bright FY spots indicating initial suberisation (arrow).

In M2 roots (see Fig. 7D1-2), cortical cells were well expanded under control conditions (D1), and roots also showed a defined endodermis, an organised pericycle and differentiated vascular tissues showing a developing vascular cambium (ca) between the xylem and the phloem. Under water deficit conditions (D2), organisation of cortical cells remained comparable but cells appeared more irregular and the cortex area was smaller (Table S5). The endodermis appeared similarly structured and more compact, while the pericycle was unchanged. By contrast, the vascular cambium disappeared, the phloem was less distinct, and the xylem development advanced. Overall, water restriction primarily affected cortical, endodermal and vascular tissues. The M2 genotype exhibited strong suberisation under water limitation. While small bright FY spots were visible between the endodermis cells in control samples (arrow Fig. 7D3), suberisation was almost complete under water-limiting conditions (Fig. 7D4), with the FY signal visible around all endodermis cell walls, particularly between cells (arrow).

In M4 roots (see Fig. 7E1-2), cortical cells were well expanded under control conditions (see left), with a defined endodermis and an organised pericycle. Vascular tissues were well differentiated, showing peripheral phloem and central xylem. Under water deficit conditions, cortex and stele areas, as well as pericycle thickness, decreased (Table S5). Cortical organisation remained similar, but cells were slightly irregular. The endodermis was less defined, suggesting reduced differentiation. Meanwhile, the pericycle became thinner. Phloem structure remained comparable, whereas xylem development appeared delayed. Overall, water deprivation primarily affected cortical, endodermal and xylem tissues. The M4 rootstock exhibited a suberisation pattern similar to M2 (see Fig. 7E3-4). Control endodermis cells showed limited suberisation (Fig. 7E3), whereas water deprivation enhanced suberin deposition around all endodermis cell walls, with a clear FY signal (see arrow in Fig. 7E4).

3.5. Salt stress

In 140 Ruggeri, cortical cells (c) under control conditions (Fig. 8A1) were well expanded, with a clearly defined endodermis (e) and an organized pericycle (pe). Vascular tissues were differentiated, with central xylem (x) and peripheral phloem (p). Under salt stress (Fig. 8A2), cortical organization remained similar, whereas the endodermis appeared more evident and strongly stained, possibly suggesting enhanced barrier function. The pericycle thinned under salt stress (Table S5). Phloem definition was reduced, and xylem elements appeared less expanded, indicating altered vascular development under salinity. Overall, salt stress primarily affected the endodermal and vascular tissues of Ruggeri 140 roots. As with water deficit conditions, Ruggeri 140 did not exhibit significant suberin deposition under salt stress. Unlike the control condition (Fig. 8A3), where the FY signal was completely absent, suberisation began in the stressed condition (Fig. 8A4). However, only small suberin spots were visible between the endodermis cells (see arrow).

In the roots of Dog Ridge plants grown under control conditions (see Fig. 8B1), the cortical cells were well expanded, and the histological sections displayed a modestly defined endodermis and an organised pericycle. Vascular tissues exhibited the characteristic arrangement of peripheral phloem and central xylem. Under salt stress (Fig. 8B2), the organisation of the cortex remained similar, with slightly larger cortical cells causing an increase in cortex area (Table S5). The endodermis appeared similar to the control condition, and the pericycle showed no structural changes. The phloem structure remained similar, whereas the xylem elements appeared less pronounced, though there were no major alterations. Overall, salt stress induced only minor anatomical changes, primarily affecting the cortical and xylem tissues. This indicates that there was limited structural adjustment in the roots of plants grown in Dog Ridge. Salt stress did not affect suberin lamellae deposition in Dog Ridge; both the control samples (Fig. 8B3) and the salt-stressed samples (Fig. 8B4) showed limited deposition with no notable differences.

In Kober 5BB roots, cortical cells under control conditions (Fig. 8C1) were well expanded, with a weakly differentiated endodermis and an organized pericycle. Vascular tissues were distinguishable, with peripheral phloem and poorly expanded central xylem. Under salt stress (Fig. 8C2), cortical organization remained similar, while the endodermis appeared less evident and more compact, suggesting reduced barrier function. The cortex and stele areas, as well as the pericycle thickness, appear larger under salt stress (Table S5). Phloem appeared comparable or slightly more expanded than in the control, and xylem appeared more developed. Overall, salinity mainly affected endodermal and vascular differentiation in Kober 5BB roots. Although histological analysis did not reveal specific endodermis cell differentiation, Kober 5BB did exhibit increased suberin lamella formation (Fig. 8C4), in the form of suberin deposition between cells (indicated by arrows), which is similar to that observed under water deficit. No suberin deposition was noted in control samples (Fig. 8C3).

Under control conditions, the cortical cells of M2 roots (Fig. 8D1) were well expanded, and the root sections clearly showed a defined endodermis and an organised pericycle. The vascular tissues were well differentiated, with central xylem and peripheral phloem. Under salt stress (Fig. 8D2), the organisation of the cortex remained similar, while the endodermis appeared locally irregular, suggesting altered barrier properties. While the cortex area increased, the stele area decreased. This changed the ratio of cortex to stele area to total area (Table S5). The pericycle appeared thinner. The phloem structure was comparable to the control, but xylem development was slightly reduced. Overall, salinity induced minor anatomical alterations, primarily impacting the

endodermal and vascular tissues of the M2 roots. Notably, under salt stress (Fig. 8D4), suberisation of the endodermis cell walls remained similar to that observed in control plants (Fig. 8D3), with locally intense FY-stained suberin present (indicated by the arrows). This contrasts with the results of the water deficit experiment.

Under control conditions, the cortical cells of M4 roots (Fig. 8E1) were well expanded, and the roots were characterised by a clearly defined endodermis and an organised pericycle. Vascular tissues showed normal differentiation, with central xylem and peripheral phloem. Under salt stress (Fig. 8E2), the organisation of the cortex remained similar, while the endodermis appeared locally irregular and compressed. The pericycle exhibited significant structural alterations, while the phloem and xylem were comparable to the control. Overall, salinity primarily impacted the endodermis and pericycle, suggesting structural adaptations related to the salt stress response. Additionally, the M4 rootstock exhibited significant suberin deposition under salt stress, with the cell border heavily stained by FY (see Fig. 8E4 and the arrow). By contrast, the endodermis cell walls of control plants showed no or a barely visible FY signal (see Fig. 8E3). The response of endodermis cells in the M4 rootstock was consistent across water deficit and salt stress experiments. Both stressed plants showed well-defined FY staining along the entire cell wall.

Full images of both the histological and fluorescence staining are provided in Supplementary Materials S5–S9. Measurements relating to the total area (A_{tot}), stele area (A_{stele}), cortex area (A_{cortex}), pericycle thickness, the ratio of the cortex to the stele and the ratio of the stele to the total area, as carried out on the histological images, are provided in Tables S5 and S6.

4. Discussion

Overall, our results demonstrate that water deficit and salinity induce similar leaf-level responses in grapevine rootstocks, characterised by reduced stomatal conductance and lower carbon assimilation. However, this phenotypic convergence was not reflected in a shared regulatory pattern at the upstream level. Under water deficit conditions, a decline in gas exchange was generally associated with strong, genotype-dependent increases in leaf abscisic acid (ABA), whereas under salinity, comparable physiological limitations developed alongside much weaker or inconsistent ABA accumulation. These findings suggest that different stress-control architectures can result in similar functional outcomes. Drought appears to be more closely linked to hormonal regulation, whereas salinity is more consistent with a greater contribution from non-hormonal constraints. In this context, rootstock differences reflected both stress sensitivity and how genotypes integrated leaf signaling with root traits to balance water conservation and photosynthesis under stress.

4.1. During water deficit, ABA content contribute to regulate the stomatal response

Although the role of abscisic acid (ABA) in grapevine stomatal closure during water deficit is well-studied, the relative importance of hormonal and hydraulic signals remains debated. Our data show that water deficit significantly increases leaf ABA content in a genotype-dependent manner across five rootstocks, with substantial accumulation observed in the Dog Ridge, Kober 5BB, M2 and M4 varieties. These results reinforce the pivotal regulatory role of ABA in the grapevine response to drought. (Marusig and Tombesi, 2020). The established model proposes that drought triggers the synthesis of ABA in the roots or leaves, which is then transported to the guard cells. This induces stomatal closure via turgor loss and reduced aperture (Galbiati et al., 2011). While strong ABA accumulation was observed in our drought-stressed plants, recent studies suggest ABA may not immediately trigger stomatal closure; Tombesi et al. (2015) found that ABA levels in *Vitis vinifera* cultivars Sangiovese and Montepulciano increased after stomatal closure. Stomatal regulation during water deficit appears also driven by passive hydraulic mechanisms, not ABA signalling. Rewatering plants after ABA peaks failed to reopen stomata, indicating ABA maintains, rather than initiates, long-term closure. This decoupling of ABA accumulation and stomatal closure is supported by observations in the 140 Ruggeri genotype, which showed reduced stomatal conductance without increased leaf ABA. Rodrigues et al. (2008) found a strong correlation between pre-dawn water potential and stomatal conductance in grapevine, suggesting stomata primarily responds to plant water status. Initially, xylem sap ABA concentrations did not correlate with stomatal conductance, suggesting hydraulic signals were primary (Rodrigues et al., 2008). However, recent research on grapevine rootstocks 1103P and 101-14MGt demonstrates distinct drought responses linked to ABA content (Bianchi et al., 2023). 1103P avoided stress via increased root ABA, reduced stomatal conductance, and inhibited photosynthesis, while 101-14MGt tolerated drought by maintaining photosynthesis (Bianchi et al., 2023). Genotypic variation in ABA accumulation (pronounced in M4 and Dog Ridge, minimal in 140 Ruggeri) correlates with stomatal control strategies. These data support a model where stomatal regulation under drought results from combined hydraulic and chemical signals, with relative contributions varying by stress severity, genotype, and environment (Rodrigues et al., 2008; Tombesi et al., 2015; Morabito et al., 2025).

4.2. Under salt stress, leaf behaviour convergence does not imply signal identity

Our study found that, despite similar reductions in stomatal conductance and CO_2 assimilation across rootstocks, physiological and hormonal responses to salinity differed significantly from those under water deficit. This challenges the assumption that similar leaf phenotypes share regulatory pathways, supporting that distinct signaling systems can yield similar functional outcomes (Cramer, 2010). While water deficit strongly induced ABA accumulation, salinity induced weaker or no ABA response, except in 140 Ruggeri, which consistently showed high ABA levels. Hormonal changes differ between salt- and drought-stressed plants, even with similar gas exchange. Previous research indicates that ABA accumulation does not always correlate with stomatal behavior under salinity, with the relative importance of ABA-dependent and -independent pathways varying by stress type (Cramer, 2010). In grapevines, salinity triggers a variety of responses, including ion transport, osmotic adjustment and signalling of oxidative stress. In this context, ABA appears to be permissive rather than instructive (Marusig and Tombesi, 2020; Galbiati et al., 2011). Unlike water deficit, which primarily causes dehydration and triggers ABA-mediated hydraulic regulation, salinity presents a dual stress: osmotic reduction of water availability and ionic toxicity from Na^+ and Cl^- accumulation (Munns and Tester, 2008). Stomatal regulation is profoundly affected by salt stress. Initial reductions in stomatal conductance are often osmotic, independent of ABA, while ion toxicity can further impair photosynthesis (Cramer, 2010). We observed instances where net CO_2 assimilation decreased more than stomatal conductance, indicating non-stomatal limitations likely due to ion accumulation or photosynthetic damage. In literature, salt stress response is frequently associated with ion transport systems (e.g., HKT and NHX transporters). In our conditions, the decline in gas exchange without significant ABA induction suggests that non-hormonal factors (potentially including ionic or osmotic constraints) might play a prevalent role, though tissue ion profiling would be required to confirm this hypothesis (Cramer, 2010; Lu et al., 2022; Tombesi et al., 2015; Downton and Loveys, 1981). Our observation of low leaf ABA levels under salinity suggests stomatal limitations primarily driven by osmotic or hydraulic constraints rather than ABA accumulation, although higher-frequency ABA profiling is needed to exclude short-term transient fluctuations.

4.3. ZEP, ABA and stress signaling

Data suggest zeaxanthin epoxidase (ZEP) regulation, a key enzyme in abscisic acid (ABA) biosynthesis catalyzing zeaxanthin to violaxanthin, is more complex than previously thought (Xiong and Zhu, 2003). Two distinct immunoreactive bands (~75 and 65 kDa) observed in grapevine suggest molecular variants with differing roles. This aligns with recent findings of multiple, subfunctionalized ZEP gene copies in *Brassica napus* (Ye et al., 2024). Distinct gene pairs (BnaA07.ZEP/BnaC07.ZEP and BnaA09.ZEP/BnaC09.ZEP) are known to exhibit tissue-specific roles in ABA biosynthesis and carotenoid production (Ye et al., 2024). The observed two bands in grapevine extracts may hypothetically represent distinct gene products with specialized functions or post-translational modifications of a single protein (Cutler et al., 2010). Molecular weight differences in ZEP proteins may reflect distinct maturation, post-translational modifications, or different localization. This parallels observations in Arabidopsis, where ZEP accumulation varies by tissue and function (Xiong and Zhu, 2003). ZEP response varied by stress condition. Under water deficit, increased intensity of the 65 kDa band in leaves and roots suggests a role in abscisic acid biosynthesis, as ZEP expression is transcriptionally regulated by water deficit and contributes to root-to-shoot signaling for stomatal closure (Audran et al., 1998). This band increase may possibly indicate an isoform involved in ABA precursor production, aligning with elevated ABA levels. Strong induction of the 75 kDa band in M4 leaves indicates genotype-specific regulation. The decreased 65 kDa band in both organs under salt stress likely correlates with low ABA levels, suggesting salinity does not activate ABA biosynthesis. Although ZEP provides substrates for NCED, its role in ABA regulation is debated; studies in *Nicotiana plumbaginifolia* show ZEP is needed for precursor synthesis but does not primarily regulate ABA accumulation like NCED (Frey et al., 2006). These data indicate ZEP protein levels are not the sole determinant of ABA content, and salt stress likely inhibits the upstream biosynthetic pathway. This aligns with the view that reduced gas exchange under salinity results from osmotic, hydraulic, and ionic limitations, not hormonal signalling (Munns et al., 2010). ZEP regulation is tissue- and stress-specific, increasing under water deficit and decreasing under salt stress, indicating fine-tuned responses; furthermore, root ZEP expression during water deficit supports their role in ABA synthesis for long-distance signalling (Audran et al., 1998). Discrepancies between ZEP protein abundance and ABA levels (such as in Dog Ridge) suggest additional regulatory controls, hypothetically involving NCED activity (Iuchi et al., 2001), ABA turnover, or carotenoid availability (Cazzonelli and Pogson, 2010). The 65 and 75 kDa ZEP isoforms likely have distinct roles, evidenced by differential responses to stress (M4 with water deficit, Dog Ridge with salt). The differential accumulation of the 65 kDa and 75 kDa ZEP-reactive bands under water deficit and salt stress suggests distinct organ- and stress-dependent regulatory patterns. However, determining whether these bands correspond to distinct gene products or post-translational modifications will require detailed proteomic and functional characterization.

4.4. Root traits are a structural foundation for water management strategies

Grapevine rootstock research increasingly recognizes root anatomy and morphology as key to stress adaptation. Here, histological analyses revealed genotypic differences in root architecture and endodermal suberisation correlating with physiological responses to water deficit and salinity, supporting evidence that root system structure actively determines whole-plant stress responses (Alonso-Forn et al., 2025; Bernardo et al., 2025). Alonso-Forn et al. (2025) showed that root morphology and anatomy are key to grapevine drought tolerance. Rootstocks with higher root length density (RLD) and finer roots maintained stem water potential better under drought, while smaller xylem vessels and reduced xylem area correlated with improved water transport and faster recovery (Alonso-Forn et al., 2025). These results are consistent with our observations on M2 and M4, which revealed an increase in endodermal suberisation during the drought. This structural modification is consistent with an enhanced endodermal barrier, which may help limit apoplastic water loss. Studies reveal a trade-off between root density and water transport efficiency (Alonso-Forn et al., 2025). Comparing Merlot grafted onto 1103 Paulsen, 420A, and M2 rootstocks, Dattola et al. (2026) identified three adaptive strategies. 1103 Paulsen showed high root biomass and hydraulic conductivity, supporting active tolerance with large canopies. Conversely, M2 exhibited low root biomass but a high proportion of absorptive roots, coupled with low stomatal conductance and high water use efficiency, representing a conservative strategy (Dattola et al., 2026). Data supports this framework: drought-tolerant M2 and M4 rootstocks (enhanced suberisation) exhibited conservative physiological responses (reduced stomatal conductance, maintained photochemical efficiency, and stable biomass allocation) while 140 Ruggeri (minimal suberisation) maintained a permissive strategy with sustained gas exchange and higher root water content. The endodermis, via its Casparian strip and suberin lamellae, regulates radial water and solute movement into the stele. Barrios-Masias et al. (2015) found that grapevine rootstock responses to water stress correlate with changes in root hydraulic physiology and suberisation; increased suberisation reduced hydraulic conductivity but improved drought tolerance, likely by limiting water loss and restricting toxic ion entry. Studies on root cortical lacunae support this concept; grapevine rootstock sensitivity and recovery from drought correlate with lacunae formation and root tip function (Cuneo et al., 2021). Rootstocks developing extensive cortical aerenchyma under stress exhibited reduced hydraulic conductivity and slower recovery (Cuneo et al., 2021). The observed suberin deposition in M2, M4 and Kober 5BB supports the hypothesis that suberisation and endodermal reinforcement can limit radial water loss and preserve hydraulic integrity during drought. Dattola et al. (2026) observed that grapevine rootstocks with higher root biomass had greater hydraulic efficiency and larger canopies, while those with proportionally more absorptive roots conserved water use at the cost of growth. Our data show similar patterns: under salinity, M4 and Kober 5BB increased root and leaf biomass despite reduced water content. Conversely, 140 Ruggeri prioritized water retention over biomass investment, maintaining high root water content despite low root biomass. Dog Ridge's low leaf-to-root ratio indicates preferential root allocation under salinity, enhancing water and ion uptake (Munns and Tester, 2008). Grapevine rootstocks employ water-conservative (reduced stomatal conductance, enhanced suberisation, and maintained water use efficiency) or water-spending strategies (sustained gas exchange and higher transpiration) (Dattola et al., 2026; Gambetta et al., 2020). Our results show that rootstock strategies vary along a continuum determined by genetics and stress, rather than being fixed. M2 and M4 rootstocks represent conservative strategies with robust suberisation and efficient water use, while 140 Ruggeri employs a more water-spending strategy relying on hydraulic signaling and osmotic adjustment due to minimal suberisation and high ABA levels. Importantly, this study evaluated non-grafted rootstocks, thereby isolating their physiological, hormonal, and anatomical responses to water-limiting and salinity stress from scion-derived interference. While this approach was essential to elucidating root-specific signaling and structural adaptations, root–scion interactions in grafted grapevines warrant further validation under both controlled and field conditions.

5. Conclusions

In conclusion, this study demonstrates how convergent leaf physiological phenotypes can arise from distinct root-level regulatory mechanisms in grapevine rootstocks under water deficit and salinity stress, as summarized in Fig. 9. Under water deficit, ABA accumulation and ZEP isoform (ZEP65) regulation coordinate with root anatomical remodelling, including a compact endodermis, irregular cortex cells, and

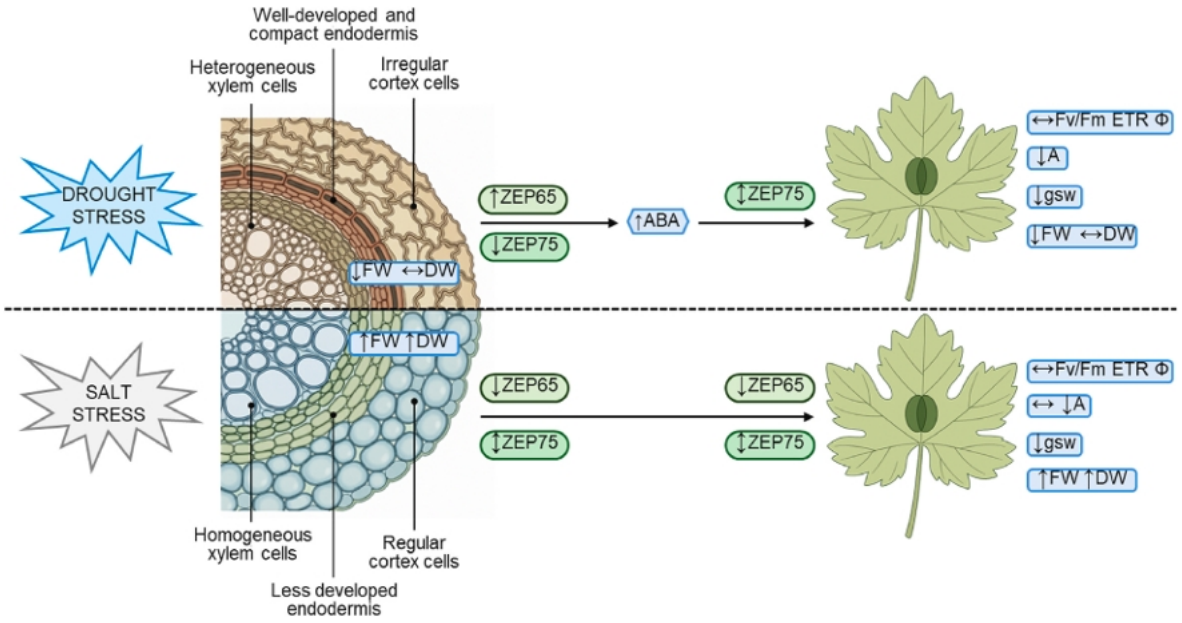

Fig. 9. Schematic representation of the divergent upstream signaling mechanisms and convergent leaf phenotypes in grapevine rootstocks under drought and salt stress. Under drought stress, leaf ABA content increases, accompanied by genotype-dependent changes in ZEP isoforms: ZEP65 generally increases, while ZEP75 shows variable responses. Gas exchange parameters (stomatal conductance, gsw; net CO_2 assimilation, A) decline, fresh weight (FW) and dry weight (DW) of leaves and roots decrease, and photosystem II efficiency (Fv/Fm, electron transport rate ETR, effective quantum yield ΦPSII) is variably affected. Root anatomical adjustments include a well-developed and compact endodermis, irregular cortex cells, and heterogeneous xylem vessels. Under salt stress, ABA accumulation is minimal or absent, ZEP65 is suppressed, and ZEP75 shows variable changes. gsw and A also decline, but biomass (FW, DW) often increases in a genotype-dependent manner. Root anatomical changes are less pronounced, with a less developed endodermis, regular cortex cells, and homogeneous xylem. Arrows indicate direction of change (↑ increase, ↓ decrease) relative to control conditions.

heterogeneous xylem, to drive conservative water use. Concurrently, plant biomass and key physiological parameters decrease. Conversely, under salt stress, minimal ABA induction and ZEP65 suppression led to less pronounced root anatomical adjustments, specifically a less developed endodermis, regular cortex cells, and homogeneous xylem. Despite these distinct anatomical and hormonal profiles, leaf physiology yields similar outcomes, demonstrating a phenotypic convergence. Additionally, while saline stress increased root and leaf biomass, it reduced CO_2 absorption and stomatal conductance.

The five genotypes examined adopted different strategies in response to water deficit and salinity, indicating that stress tolerance is not a single trait, but the outcome of various interacting mechanisms (Ollat et al., 2015). Under limited water availability, rootstocks such as M2 and M4 showed robust ABA-mediated stomatal control and inducible endodermal suberisation thereby conserving water and preserving hydraulic function (Gambetta et al., 2020). Conversely, under salinity, genotypes such as 140 Ruggeri offer advantages by sustaining gas exchange and relying less on hormonal signaling and more on osmotic adjustment and ion exclusion (Munns and Tester, 2008). The divergent response of Dog Ridge, which is moderately drought tolerant but significantly salt susceptible, highlights the risk of single factor assessment for rootstock selection. Furthermore, the aeroponic cultivation system proved to be an effective experimental tool to isolate and characterize root traits and signalling pathways regardless of soil variation. Overall, these findings highlight that leaf physiological convergence under abiotic stress hides distinct, stress-specific root anatomical and hormonal control mechanisms.

Declaration of competing interest

The authors declare that they have no known competing financial interests or personal relationships that could have appeared to influence the work reported in this paper.

Acknowledgements

The authors gratefully acknowledge the Doctoral Programme in SAFAS of the Tuscany region (https://www.phd-safas.dagri.unifi.it/index.html?newlang=eng) for supporting Sara Anichini with a PhD fellowship. Special thanks are also extended to the Santa Chiara Lab of Siena University (https://santachiaralab.unisi.it/) for providing the facilities and resources necessary to conduct this research. We would also like to thank Prof. Silvia Casini and her group at the Department of Physical, Environmental and Earth Sciences at the University of Siena for granting us access to the microplate reader used for the colorimetric assays.

Appendix A. Supplementary data

Supplementary data to this article can be found online at https://doi.org/10.1016/j.plaphy.2026.111680.

Data availability

Data will be made available on request.

References

Alonso-Forn, D., Buesa, I., Flor, L., Sabater, A., Medrano, H., Escalona, J.M., 2025. Implications of root morphology and anatomy for water deficit tolerance and recovery of grapevine rootstocks. Front. Plant Sci. 16. https://doi.org/10.3389/fpls.2025.1541523.

Atkinson, J.A., Pound, M.P., Bennett, M.J., Wells, D.M., 2019. Uncovering the hidden half of plants using new advances in root phenotyping. Curr. Opin. Biotechnol. 55, 1–8. https://doi.org/10.1016/j.copbio.2018.06.002.

Audran, C., Borel, C., Frey, A., Sotta, B., Meyer, C., Simonneau, T., Marion-Poll, A., 1998. Expression studies of the zeaxanthin epoxidase gene in *Nicotiana plumbaginifolia*. Plant Physiol. 118 (3), 1021–1028. https://doi.org/10.1104/pp.118.3.1021.

Barrios-Masias, F.H., Knipfer, T., McElrone, A.J., 2015. Differential responses of grapevine rootstocks to water stress are associated with adjustments in fine root hydraulic physiology and suberization. J. Exp. Bot. 66 (19), 6069–6078. https://doi.org/10.1093/jxb/erv324.

Bernardo, S., Marguerit, E., Ollat, N., Gambetta, G.A., Saint Cast, C., De Miguel, M., 2025. Root system ideotypes: what is the potential for breeding drought-tolerant grapevine rootstocks? J. Exp. Bot. 76 (11), 2970–2984. https://doi.org/10.1093/jxb/eraf006.

Bianchi, D., Ricciardi, V., Pozzoli, C., Grossi, D., Caramanico, L., Pindo, M., Stefani, E., Cestaro, A., Brancadoro, L., De Lorenzis, G., 2023. Physiological and transcriptomic evaluation of drought effect on own-rooted and grafted grapevine rootstock (1103P and 101-14MGt). Plants 12 (5). https://doi.org/10.3390/plants12051080.

Cazzonelli, C.I., Pogson, B.J., 2010. Source to sink: regulation of carotenoid biosynthesis in plants. Trends Plant Sci. 15 (5), 266–274. https://doi.org/10.1016/j.tplants.2010.02.003.

Chen, Y., Fei, Y., Howell, K., Chen, D., Clingeleffer, P., Zhang, P., 2024. Rootstocks for grapevines now and into the future: selection of rootstocks based on drought tolerance, soil nutrient availability, and soil pH. Aust. J. Grape Wine Res. 2024 (1), 6704238. https://doi.org/10.1155/2024/6704238.

Cramer, G.R., 2010. Abiotic stress and plant responses from the whole Vine to the genes. Aust. J. Grape Wine Res. 16, 86–93. https://doi.org/10.1111/j.1755-0238.2009.00058.x.

Cuneo, I.F., Barrios-Masias, F., Knipfer, T., Uretsky, J., Reyes, C., Lenain, P., Brodersen, C.R., Walker, M.A., McElrone, A.J., 2021. Differences in grapevine rootstock sensitivity and recovery from drought are linked to fine root cortical lacunae and root tip function. New Phytol. 229 (1), 272–283. https://doi.org/10.1111/nph.16542.

Cutler, S.R., Rodriguez, P.L., Finkelstein, R.R., Abrams, S.R., 2010. Abscisic acid: emergence of a core signaling network. Annu. Rev. Plant Biol. 61 (1), 651–679. https://doi.org/10.1146/annurev-arplant-042809-112122.

Dargie, T., Dor, A., Manuel, A., Molly, C., 2014. Responses of grapevine rootstocks to drought stress. Int. J. Plant Physiol. Biochem. 6 (1), 1–6. https://doi.org/10.5897/IJPPB2013.0199.

Dattola, A., Iuzzolini, P., Giglio Verga, F., Zappia, R., Gullo, G., 2026. Hydraulic efficiency, root allocation, and photosynthetic regulation in young grapevine rootstocks under controlled conditions. Horticulturae 12 (2), 142. https://doi.org/10.3390/horticulturae12020142.

Degenkolbe, T., Do, P.T., Zuther, E., Repsilber, D., Walther, D., Hincha, D.K., Köhl, K.I., 2009. Expression profiling of rice cultivars differing in their tolerance to long-term drought stress. Plant Mol. Biol. 69 (1–2), 133–153. https://doi.org/10.1007/s11103-008-9412-7.

Downton, W., Loveys, B., 1981. Abscisic acid content and osmotic relations of salt-stressed grapevine leaves. Aust. J. Plant Physiol. 8 (5), 443–452. https://doi.org/10.1071/PP9810443.

Fichtl, L., Hofmann, M., Kahlen, K., Voss-Fels, K.P., Cast, C.S., Ollat, N., Vivin, P., Loose, S., Nsibi, M., Schmid, J., Strack, T., Schultz, H.R., Smith, J., Friedel, M., 2023. Towards grapevine root architectural models to adapt viticulture to drought. Front. Plant Sci. 14, 1162506. https://doi.org/10.3389/fpls.2023.1162506.

Frey, A., Boutin, J.-P., Sotta, B., Mercier, R., Marion-Poll, A., 2006. Regulation of carotenoid and ABA accumulation during the development and germination of Nicotiana plumbaginifolia seeds. Planta 224 (3), 622–632. https://doi.org/10.1007/s00425-006-0231-2.

Galbiati, M., Matus, J.T., Francia, P., Rusconi, F., Cañón, P., Medina, C., Conti, L., Cominelli, E., Tonelli, C., Arce-Johnson, P., 2011. The grapevine guard cell-related VvMYB60 transcription factor is involved in the regulation of stomatal activity and is differentially expressed in response to ABA and osmotic stress. BMC Plant Biol. 11 (1), 142. https://doi.org/10.1186/1471-2229-11-142.

Gambetta, G.A., Herrera, J.C., Dayer, S., Feng, Q., Hochberg, U., Castellarin, S.D., 2020a. The physiology of drought stress in grapevine: towards an integrative definition of drought tolerance. J. Exp. Bot. 71 (16), 4658–4676. https://doi.org/10.1093/jxb/eraa245.

Gambetta, G.A., Herrera, J.C., Dayer, S., Feng, Q., Hochberg, U., Castellarin, S.D., 2020b. The physiology of drought stress in grapevine: towards an integrative definition of drought tolerance. J. Exp. Bot. 71 (16), 4658–4676. https://doi.org/10.1093/jxb/eraa245.

Hajizadeh Sisakhti, S., Dehdari, M., Ebrahimi, M.A., 2025. Responses of some important physiological traits of regenerated plantlet grape (Vitis vinifera L.) genotypes to cold stress. Discover Plants 2 (1), 120. https://doi.org/10.1007/s44372-025-00202-7.

Iuchi, S., Kobayashi, M., Taji, T., Naramoto, M., Seki, M., Kato, T., Tabata, S., Kakubari, Y., Yamaguchi-Shinozaki, K., Shinozaki, K., 2001. Regulation of drought tolerance by gene manipulation of 9- *cis* -epoxycarotenoid dioxygenase, a key enzyme in abscisic acid biosynthesis in *Arabidopsis*. Plant J. 27 (4), 325–333. https://doi.org/10.1046/j.1365-313x.2001.01096.x.

Khan, M.M., Akram, M.T., Qadri, R.W.K., Al-Yahyai, R., 2020. Role of grapevine rootstocks in mitigating environmental stresses: a review. J. Agricult. Mar. Sci. 25 (2), 1. https://doi.org/10.24200/jams.vol25iss2pp1-12 *[JAMS]*.

Koundouras, S., Tsialtas, I.T., Zioziou, E., Nikolaou, N., 2008. Rootstock effects on the adaptive strategies of grapevine (Vitis vinifera L. cv. Cabernet–Sauvignon) under contrasting water status: leaf physiological and structural responses. Agric. Ecosyst. Environ. 128 (1–2), 86–96. https://doi.org/10.1016/j.agee.2008.05.006.

Labarga, D., Mairata, A., Puelles, M., Martín, I., Albacete, A., García-Escudero, E., Pou, A., 2023. The rootstock genotypes determine drought tolerance by regulating aquaporin expression at the transcript level and phytohormone balance. Plants 12 (4), 718. https://doi.org/10.3390/plants12040718.

Lin, H.-A., Coker, H.R., Park, S., Finlayson, S.A., Tfaily, M.M., Nagy, E.M., Hague, S., Antony-Babu, S., Howe, J.A., Smith, A.P., 2024. Aeroponic approach for nondestructive root exudate collection and simulation of variable water stress trialed on cotton (Gossypium hirsutum). Sci. Rep. 14 (1), 28615. https://doi.org/10.1038/s41598-024-79801-5.

Lovisolo, C., Perrone, I., Carra, A., Ferrandino, A., Flexas, J., Medrano, H., Schubert, A., 2010. Drought-induced changes in development and function of grapevine (Vitis spp.) organs and in their hydraulic and non-hydraulic interactions at the whole-plant level: a physiological and molecular update. Funct. Plant Biol. 37 (2), 98–116. https://doi.org/10.1071/FP09191.

Lu, X., Ma, L., Zhang, C., Yan, H., Bao, J., Gong, M., Wang, W., Li, S., Ma, S., Chen, B., 2022. Grapevine (Vitis vinifera) responses to salt stress and alkali stress: transcriptional and metabolic profiling. BMC Plant Biol. 22 (1), 528. https://doi.org/10.1186/s12870-022-03907-z.

Lucini, L., Miras-Moreno, B., Busconi, M., Marocco, A., Gatti, M., Poni, S., 2020. Molecular basis of rootstock-related tolerance to water deficit in Vitis vinifera L. cv. Sangiovese: a physiological and metabolomic combined approach. Plant Sci. 299, 110600. https://doi.org/10.1016/j.plantsci.2020.110600.

Marguerit, E., Brendel, O., Lebon, E., Van Leeuwen, C., Ollat, N., 2012. Rootstock control of scion transpiration and its acclimation to water deficit are controlled by different genes. New Phytol. 194 (2), 416–429. https://doi.org/10.1111/j.1469-8137.2012.04059.x.

Marín, D., Armengol, J., Carbonell-Bejerano, P., Escalona, J.M., Gramaje, D., Hernández-Montes, E., Intrigliolo, D.S., Martínez-Zapater, J.M., Medrano, H., Mirás-Avalos, J. M., Palomares-Rius, J.E., Romero-Azorín, P., Savé, R., Santesteban, L.G., De Herralde, F., 2021. Challenges of viticulture adaptation to global change: tackling the issue from the roots. Aust. J. Grape Wine Res. 27 (1), 8–25. https://doi.org/10.1111/ajgw.12463.

Marusig, D., Tombesi, S., 2020. Abscisic acid mediates drought and salt stress responses in Vitis vinifera—A review. Int. J. Mol. Sci. 21 (22), 8648. https://doi.org/10.3390/ijms21228648.

Meggio, F., Pitacco, A., 2016. Effect of water and salt stress on energy partitioning of two grapevine rootstock genotypes: a quantitative assessment. Acta Hortic. (1136), 121–128. https://doi.org/10.17660/ActaHortic.2016.1136.17.

Meggio, F., Prinsi, B., Negri, A.S., Simone Di Lorenzo, G., Lucchini, G., Pitacco, A., Failla, O., Scienza, A., Cocucci, M., Espen, L., 2014. Biochemical and physiological responses of two grapevine rootstock genotypes to drought and salt treatments: response of two genotypes to drought and salinity. Aust. J. Grape Wine Res. 20 (2), 310–323. https://doi.org/10.1111/ajgw.12071.

Migliaro, D., De Lorenzis, G., Di Lorenzo, G.S., De Nardi, B., Gardiman, M., Failla, O., Brancadoro, L., Crespan, M., 2019. Grapevine Non- *vinifera* genetic diversity assessed by simple sequence repeat markers as a starting point for new rootstock breeding programs. Am. J. Enol. Vitic. 70 (4), 390–397. https://doi.org/10.5344/ajev.2019.18054.

Moshelion, M., Dietz, K.-J., Dodd, I.C., Muller, B., Lunn, J.E., 2024. Guidelines for designing and interpreting drought experiments in controlled conditions. J. Exp. Bot. 75 (16), 4671–4679. https://doi.org/10.1093/jxb/erae292.

Munns, R., Tester, M., 2008. Mechanisms of salinity tolerance. Annu. Rev. Plant Biol. 59 (1), 651–681. https://doi.org/10.1146/annurev.arplant.59.032607.092911.

Munns, R., Wallace, P.A., Teakle, N.L., Colmer, T.D., 2010. Measuring soluble ion concentrations (Na+, K+, cl−) in salt-treated plants. In: Sunkar, R. (Ed.), Plant Stress Tolerance, 639. Humana Press, pp. 371–382. https://doi.org/10.1007/978-1-60761-702-0_23 (A c. Di).

Mustapha, A., Hakeem, A., Li, S., Mustafa, G., Elatafi, E., Fang, J., Zhou, C., 2025. Grapevine rootstocks and salt stress tolerance: mechanisms, omics insights, and implications for sustainable viticulture. Int. J. Plant Biol. 16 (4), 129. https://doi.org/10.3390/ijpb16040129.

Ollat, N., Peccoux, A., Papura, D., Esmenjaud, D., Marguerit, E., Tandonnet, J.-P., Bordenave, L., Cookson, S.J., Barrieu, F., Rossdeutsch, L., Lecourt, J., Lauvergeat, V., Vivin, P., Bert, P.-F., Delrot, S., 2015. Rootstocks as a component of adaptation to environment. In: Gerós, H., Chaves, M.M., Gil, H.M., Delrot, S. (Eds.), Grapevine in a Changing Environment, 1a ed. Wiley, pp. 68–108. https://doi.org/10.1002/9781118735985.ch4 (A c. Di).

Parri, S., Faleri, C., Romi, M., Del Río, J.C., Rencoret, J., Dias, M.C.P., Anichini, S., Cantini, C., Cai, G., 2024. Unravelling different water management strategies in three olive cultivars: the role of osmoprotectants, proteins, and wood properties. Int. J. Mol. Sci. 25 (20), 11059. https://doi.org/10.3390/ijms252011059.

Pizzio, G.A., Mayordomo, C., Illescas-Miranda, J., Coego, A., Bono, M., Sanchez-Olvera, M., Martin-Vasquez, C., Samantara, K., Merilo, E., Forment, J., Estevez, J.C., Nebauer, S.G., Rodriguez, P.L., 2024. Basal ABA signaling balances transpiration and photosynthesis. Physiol. Plantarum 176 (5), e14494. https://doi.org/10.1111/ppl.14494.

Prinsi, B., Muratore, C., Espen, L., 2021. Biochemical and proteomic changes in the roots of m4 grapevine rootstock in response to nitrate availability. Plants 10 (4). https://doi.org/10.3390/plants10040792.

Qin, L., Kang, W., Qi, Y., Zhang, Z., Wang, N., 2016. The influence of silicon application on growth and photosynthesis response of salt stressed grapevines (Vitis vinifera L.). Acta Physiol. Plant. 38 (3), 68. https://doi.org/10.1007/s11738-016-2087-9.

Rius-Garcia, X., Videgain-Marco, M., Casanova-Gascón, J., Acuña-Rello, L., Martín-Ramos, P., 2025. Physiological response to salinity in novel M-Series grapevine rootstocks: a comparison with commercial standards. Agronomy 15 (2). https://doi.org/10.3390/agronomy15020473.

Rodrigues, M.L., Santos, T.P., Rodrigues, A.P., De Souza, C.R., Lopes, C.M., Maroco, J.P., Pereira, J.S., Chaves, M.M., 2008. Hydraulic and chemical signalling in the regulation of stomatal conductance and plant water use in field grapevines growing under deficit irrigation. Funct. Plant Biol. 35 (7), 565–579. https://doi.org/10.1071/FP08004.

Tafesse, E.G., Aidoo, M.K., Lazarovitch, N., Rachmilevitch, S., 2021. Aeroponic systems: a unique tool for estimating plant water relations and NO_3 uptake in response to salinity stress. Plant Direct 5 (4), e00312. https://doi.org/10.1002/pld3.312.

Tombesi, S., Nardini, A., Frioni, T., Soccolini, M., Zadra, C., Farinelli, D., Poni, S., Palliotti, A., 2015. Stomatal closure is induced by hydraulic signals and maintained by ABA in drought-stressed grapevine. Sci. Rep. 5 (1), 12449. https://doi.org/10.1038/srep12449.

Tramontini, S., Van Leeuwen, C., Domec, J.-C., Destrac-Irvine, A., Basteau, C., Vitali, M., Mosbach-Schulz, O., Lovisolo, C., 2013. Impact of soil texture and water availability on the hydraulic control of plant and grape-berry development. Plant Soil 368 (1–2), 215–230. https://doi.org/10.1007/s11104-012-1507-x.

Tregeagle, J.M., Tisdall, J.M., Tester, M., Walker, R.R., 2010. Cl– uptake, transport and accumulation in grapevine rootstocks of differing capacity for cl–-exclusion. Funct. Plant Biol. 37 (7), 665–673. https://doi.org/10.1071/FP09300.

Trenti, M., Lorenzi, S., Bianchedi, P.L., Grossi, D., Failla, O., Grando, M.S., Emanuelli, F., 2021. Candidate genes and SNPs associated with stomatal conductance under drought stress in Vitis. BMC Plant Biol. 21 (1), 7. https://doi.org/10.1186/s12870-020-02739-z.

Vandeleur, R.K., Mayo, G., Shelden, M.C., Gilliham, M., Kaiser, B.N., Tyerman, S.D., 2009. The role of plasma membrane intrinsic protein aquaporins in water transport through roots: diurnal and drought stress responses reveal different strategies between isohydric and anisohydric cultivars of grapevine. Plant Physiol. 149 (1), 445–460. https://doi.org/10.1104/pp.108.128645.

Wu, X., Gong, F., Wang, W., 2014. Protein extraction from plant tissues for 2DE and its application in proteomic analysis. Proteomics 14 (6), 645–658. https://doi.org/10.1002/pmic.201300239.

Xiong, L., Zhu, J.-K., 2003. Regulation of abscisic acid biosynthesis. Plant Physiol. 133 (1), 29–36. https://doi.org/10.1104/pp.103.025395.

Ye, S., Huang, Y., Ma, T., Ma, X., Li, R., Shen, J., Wen, J., 2024. BnaABF3 and BnaMYB44 regulate the transcription of zeaxanthin epoxidase genes in carotenoid and abscisic acid biosynthesis. Plant Physiol. 195 (3), 2372–2388. https://doi.org/10.1093/plphys/kiae184.

Zhang, J., Nai, G., Li, Z., Qin, X., Li, S., Ma, S., 2026. Salt tolerance evaluation of 15 grape germplasm and screening of salt-tolerant resources. Russ. J. Plant Physiol. 73 (3), 128. https://doi.org/10.1134/S1021443726600455.

Zhang, L., Marguerit, E., Rossdeutsch, L., Ollat, N., Gambetta, G.A., 2016. The influence of grapevine rootstocks on scion growth and drought resistance. Theor. Exp. Plant Physiol. 28 (2), 143–157. https://doi.org/10.1007/s40626-016-0070-x.

Zhou-Tsang, A., Wu, Y., Henderson, S.W., Walker, A.R., Borneman, A.R., Walker, R.R., Gilliham, M., 2021. Grapevine salt tolerance. Aust. J. Grape Wine Res. 27 (2), 149–168. https://doi.org/10.1111/ajgw.12487.